Autogenous deformation-induced stress evolution in cementitious materials considering viscoelastic properties

A review of experiments and models

Liang, Minfei; Xie, Jinbao; He, Shan; Chen, Yu; Schlangen, Erik; Šavija, Branko

DOI
10.1016/j.dibe.2024.100356

Publication date
2024

Document Version
Final published version

Published in
Developments in the Built Environment

Citation (APA)
Liang, M., Xie, J., He, S., Chen, Y., Schlangen, E., & Šavija, B. (2024). Autogenous deformation-induced stress evolution in cementitious materials considering viscoelastic properties: A review of experiments and models. *Developments in the Built Environment*, *17*, Article 100356. https://doi.org/10.1016/j.dibe.2024.100356

Developments in the Built Environment 17 (2024) 100356

Contents lists available at ScienceDirect

Developments in the Built Environment

journal homepage: www.sciencedirect.com/journal/developments-in-the-built-environment

Autogenous deformation-induced stress evolution in cementitious materials considering viscoelastic properties: A review of experiments and models

Minfei Liang *, Jinbao Xie, Shan He, Yu Chen, Erik Schlangen, Branko Šavija

Microlab, Faculty of Civil Engineering and Geosciences, Delft University of Technology, Delft, 2628 CN, the Netherlands

ARTICLE INFO

Keywords:
Cementitious materials
Early-age cracking
Autogenous deformation
Elastic modulus
Creep
Relaxation
Stress evolution

ABSTRACT

Early-age cracking risk induced by autogenous deformation is high for cementitious materials of low water-binder ratios. The autogenous deformation, viscoelastic properties, and stress evolution are three important factors for understanding and quantifying the early-age cracking risk. This paper systematically reviewed the experimental and modelling techniques of the three factors. It is found that the Temperature Stress Testing Machine is a unified experimental method for all these three factors, with a strain-controlled mode for stress evolution, hourly-repeated loading scheme for viscoelastic properties, and free condition for autogenous deformation. Such unified method provides basis for developing various models. By coupling a hydration model for volume fractions of hydrates, a homogenization model for upscaling of viscoelastic properties, and capillary pressure theory for self-desiccation shrinkage, a unified model directly mapping the mix design to the early-age stress can be constructed, which can help optimize the mix design to reduce the early-age cracking risk.

1. Introduction

Early-age cracking (EAC) is a common issue encountered during the construction of concrete structures, which not only results in financial losses for contractors but also compromises the durability and aesthetics of the structures. As shown in Fig. 1, EAC is caused by a combination of early-age behaviors and properties of cementitious materials, including restrained volumetric deformation and mechanical properties, which are influenced by mixture design and environmental factors (Maruyama and Lura, 2019; Safiuddin et al., 2018). When the volumetric deformation of hardening concrete is restrained, e.g., by adjacent structures, early-age stress (EAS) builds up in the young concrete, potentially resulting in EAC if the EAS exceeds the material's tensile strength. The development of strength can be reliably determined via standard testing methods; however, acquiring EAS data presents a more challenging aspect of risk assessment in EAC, and is therefore the main focus of many EAC studies (Fairbairn and Azenha, 2019). In the EAS evolution process, the restrained volumetric deformation is the root cause, while the mechanical properties determine the rate of EAS buildup per restrained deformation. Therefore, it is necessary to consider the restrained volumetric deformation and mechanical properties as inputs in order to calculate the EAS for evaluation of the EAC risk (Bentur and Kovler, 2003).

The volumetric deformation relevant to EAC mainly includes thermal, drying, and autogenous deformation. Thermal deformation is induced during the heat release of hydration reaction and the heat transfer between the concrete structures and the environment. Due to the low thermal conductivity of concrete, the heat released by the hydration reaction of cementitious materials accumulates within concrete structures in the beginning and afterward slowly dissipates into the environment, resulting in a heating and cooling process that leads to thermal deformation (Klemczak and Żmij, 2019). Massive structures are more prone to EAC induced by thermal deformation because the heat dissipates more slowly, which results in fast temperature increase in first two days of hydration and longer cooling process afterward. Such cooling process induces negative thermal strains and further results in tensile EAS that can cause EAC. Numerous strategies have been proven to effectively ease thermal deformation, such as the use of supplementary cementitious materials (SCMs) to reduce the total hydration heat (Safiuddin et al., 2018; Xin et al., 2022).

Drying shrinkage is induced by the moisture transfer between the concrete structure and the environment. It is generally believed that the moisture loss causes a decrease of internal RH, produces capillary pressure to compress the microstructure, and leads to apparent drying

* Corresponding author.
E-mail addresses: M.Liang-1@tudelft.nl (M. Liang), J.Xie-1@tudelft.nl (J. Xie), S.He-2@tudelft.nl (S. He), Y.Chen-6@tudelft.nl (Y. Chen), Erik.Schlangen@tudelft.nl (E. Schlangen), B.Savija@tudelft.nl (B. Šavija).

https://doi.org/10.1016/j.dibe.2024.100356
Received 13 October 2023; Received in revised form 28 December 2023; Accepted 30 January 2024
Available online 7 February 2024

shrinkage observed at the macroscale (Huang et al., 2021). Other mechanisms are also involved in the drying deformation, including changes in surface free energy, disjoining pressure, and interlayer water movement (Tran et al., 2021). Contrary to the thermal deformation, EAC induced by drying deformation is less pronounced in massive structures because the moisture loss mostly occurs in the superficial layer of the structure, while it proceeds much more slowly in the core. Moreover, proper curing can effectively alleviate drying shrinkage at an early age by preventing moisture loss from the material to the environment (Yang et al., 2017).

The thermal and drying deformation depend not only on the material itself but also significantly on structural size and the environment, as heat and moisture transfer play a dominant role in inducing these deformations. In contrast, autogenous deformation (AD) is a material behavior that is not related to any substance exchange between the structure and environment. AD mainly arises from the consumption of pore water by the hydration reaction, also known as "self-desiccation", and directly relates to the hydration of the cementitious material utilized (Hu et al., 2013). The advancement of modern construction industries tends to use greener cementitious materials with high performance, which significantly affect AD and therefore the risk of EAC. For example, high-performance concrete (HPC) and ultra-high-performance concrete (UHPC) have a significantly higher risk of EAC regarding AD due to lower water/binder ratios and the incorporation of silica fume (Wu et al., 2017; Yang et al., 2019; Zhang et al., 2019a). Furthermore, concrete that uses high-volume slag or alkali-activated binders, which aim to replace the Ordinary Portland Cement (OPC) has and reduce its high carbon emission, shows a much higher EAC risk because of more significant AD (Zhang et al., 2022a; Liang et al., 2023a).

Various experimental methods have been developed to mitigate the high EAC risk induced by AD (Hu et al., 2013). However, among these tests, the timing at which the measurement should be started, referred to as "time-zero", has always been a debatable issue (Darquennes et al., 2011a; Filho et al., 2019). In view of the time-zero issue, a corrugated tube test is commonly used because it is both convenient and accurate, and allows the test to start immediately after placement of fresh mixture (Wyrzykowski et al., 2017). In addition to experimental methods, multiple analytical models have also been proposed to predict AD (Tang et al., 2021), most of which are based on the capillary tension theory. Furthermore, several mitigation strategies have been advised to reduce AD, including internal curing (by superabsorbent polymers, lightweight aggregate, and recycled concrete aggregate), control of hydration reaction, formation of expansive products, and use of shrinkage-reducing admixtures (Yang et al., 2019; Schröfl et al., 2022; Mao et al., 2021; Klausen and Kanstad, 2021; Zhan and He, 2019; Zhang et al., 2022b; Moelich et al., 2022). Nevertheless, as shown in Fig. 1, restrained AD is the root cause of EAS evolution, while material properties (especially viscoelastic properties) determine the rate of EAS accumulation per AD. Therefore, only knowing the AD is not sufficient to predict the EAS; hence, the EAC risk cannot be accurately quantified (Bentur and Kovler, 2003).

As the combined result of restrained AD and mechanical properties of hardening cementitious materials, EAS is a straightforward indicator to evaluate the EAC risk (Zhu et al., 2021). To quantify the EAS, several testing methods have been devised to measure the EAS evolution when the volumetric deformation is restrained, including the ring test, plate test, longitudinal test, and substrate restraint test (Bentur and Kovler, 2003; Xin et al., 2020; Serdar et al., 2020). Among these tests, the Temperature-Stress-Testing-Machine (TSTM) stands out with advantages in explicit and flexible mechanical loading schemes, active temperature control, and tunable restraint degree (Staquet et al., 2012), which allow for a wide range of early-age tests for tensile and compressive creep, elastic modulus, and coefficients of thermal expansion and contraction (Nguyen et al., 2019). In addition, different modelling schemes have been developed to simulate the EAS evolution using analytical or numerical methods (Klausen, 2016; Liu and Schindler, 2020; Liang et al., 2022a,b). These models use the measured AD and viscoelastic properties as input to run simulations following a constitutive relationship of linear viscoelasticity. While most models have proved effective for simulating EAS using linear viscoelasticity, they strongly rely on the measured AD and viscoelastic properties (i.e., elastic modulus and aging creep/relaxation). The costs, reliability, and complexity of these early-age tests, including tests for AD, creep, and EAS, hinder a thorough parametric study which requires numerous experimental efforts. Thus, understanding the mechanisms behind these material behaviors/properties and setting up corresponding modelling schemes are important for the better evaluation of AD-induced EAC risk.

To summarize, the EAC is a complex issue concerning a blend of multi-field and multi-scale mechanisms related to hydration of cementitious materials, heat transport, moisture transport, and solid mechanics (including micromechanical analysis for homogenization of material properties, viscoelastic analysis for stress evolution, and damage analysis for high-stress level conditions). Studies (Fairbairn and Azenha, 2019; Serdar et al., 2020) have provided a comprehensive overview on the recent development of experimental and modelling techniques for this issue. Acknowledging the significance of EAC induced by AD, this paper aims to provide a more concise overview of EAC induced by AD. Following the logic presented by Fig. 2, this paper highlights that AD and viscoelastic properties are necessary input for calculating the stress evolution, and provides details of the state-of-the-art experimental and modelling techniques for 1) obtaining autogenous deformation and viscoelastic properties and then 2) obtaining the stress evolution, which then can lay basis for building an end-to-end (i.e., from mix and environmental results to stress) experimental or modelling scheme for the understanding of EAS evolution induced by AD.

The structure of this paper is shown in Fig. 2. This paper focuses on experimental and modelling techniques of AD, viscoelastic properties,

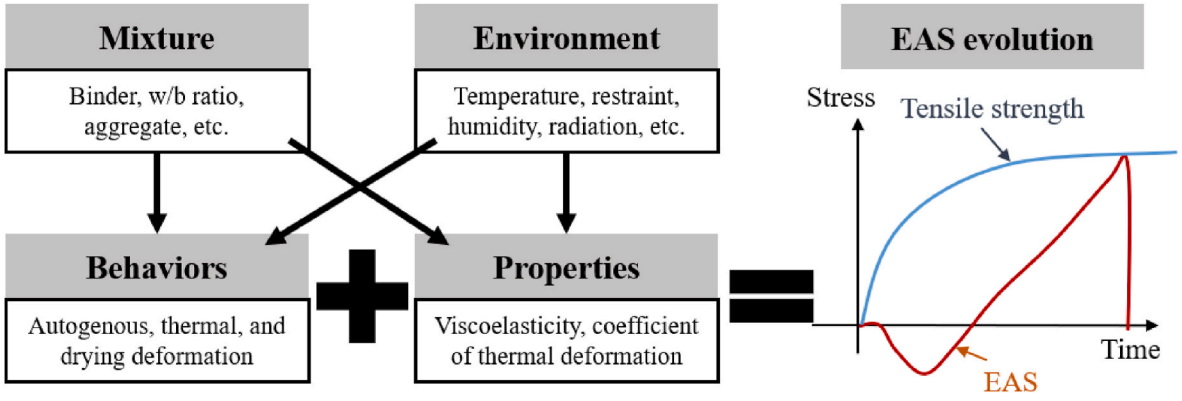

Fig. 1. Schematic figure for early age stress buildup and EAC.

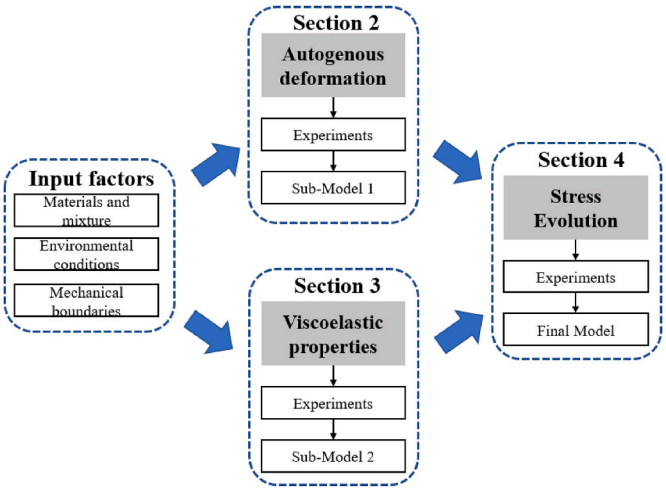

Fig. 2. Structure of the paper.

and their combined effect, i.e., the EAS evolution in early-age cementitious materials. The experimental analysis is the basis of the modelling technique, and therefore is introduced at the beginning of each section. Sections 2 and 3 introduce the AD and viscoelastic properties. Then section 4 summarizes the studies of the EAS which should be analyzed in combination with AD and viscoelastic properties in previous 2 sections. With the aim to build an end-to-end model for EAC prevention (i.e., from mixture to the EAS), the sub-model 1 in Section 2 for AD prediction and sub-model 2 in Section 3 for prediction of viscoelastic properties should be used as the input for the final model in Section 4 to predict EAS with a linear viscoelastic constitutive relationship.

2. Autogenous deformation

Autogenous deformation (AD) ε_{ad} refers to volumetric deformation produced by continuous hydration of cementitious materials, excluding the effects of applied load and changes in either temperature or moisture (American Concrete Institute, 2008). As shown by Fig. 3, AD mainly comprises two parts: the autogenous swelling ε_{sw} and self-desiccation shrinkage ε_{sd}. Furthermore, if the temperature of the concrete is not constant, the apparent AD includes the thermal deformation ε_{th}. The chemical shrinkage happens before the solid skeleton formation, i.e., when the microstructure is not rigid enough to induce any EAS, and therefore chemical shrinkage can be neglected in many EAC analyses (Wu et al., 2017). In comparison, self-desiccation refers to the pore water consumption by continuous hydration after the solid skeleton is formed. Following the theory of capillary pressure (Lura et al., 2003), water consumption causes a drop in internal relative humidity (RH), induces capillary pressure to compress the pore structure, and finally leads to overall volume contraction. If the self-desiccation shrinkage is restrained, considering the stiffness of the solid structure, tensile stress can be generated and thus poses the EAC risk. Another part of AD, the autogenous swelling, happens mainly because of the chemo-mechanical couplings between expansive hydration products (e.g., ettringite) and the pore structure (Barcelo et al., 2005; Carette and Staquet, 2018; Carette et al., 2018). The production of ettringite causes an initial expansion and therefore compressive stress in restrained concrete, which delays the development of tensile stress and reduces EAC risk (Liang et al., 2023a). However, autogenous swelling is often neglected or underestimated (Tang et al., 2021), potentially because many AD tests start too late, ranging from 1 day to several days, which may directly skip the part of autogenous swelling (Carette et al., 2018). Another reason may be that the generation of expansive products depends highly on cement chemistry, such as the content of C3A and gypsum, and only certain cements generate enough expansive products to induce apparent expansion. Furthermore, thermal deformation, which often leads to expansion and shrinkage, also makes it difficult to identify the "true" autogenous swelling and self-desiccation shrinkage (Orosz et al., 2017).

2.1. Experiments for autogenous deformation

2.1.1. Methods

Following the definition of AD, the test needs to be performed with strict sealing and temperature control. The sealing condition is to prevent moisture loss of the specimen and to exclude drying deformation, while temperature should prevent thermal deformation and changes in hydration kinetics that can be induced by temperature variation in the specimen. The most common way to test AD is to measure the length change of prismatic or cylindrical specimens with length sensors such as Linear Variable Differential Transformers (LVDT) or laser transducers attached at the side of the specimen (Staquet et al., 2012; Amin et al., 2010) or strain transducers embedded in the core of the specimen (Zhang et al., 2003). As a contactless measurement method, laser transducers provide several advantages, including a more convenient

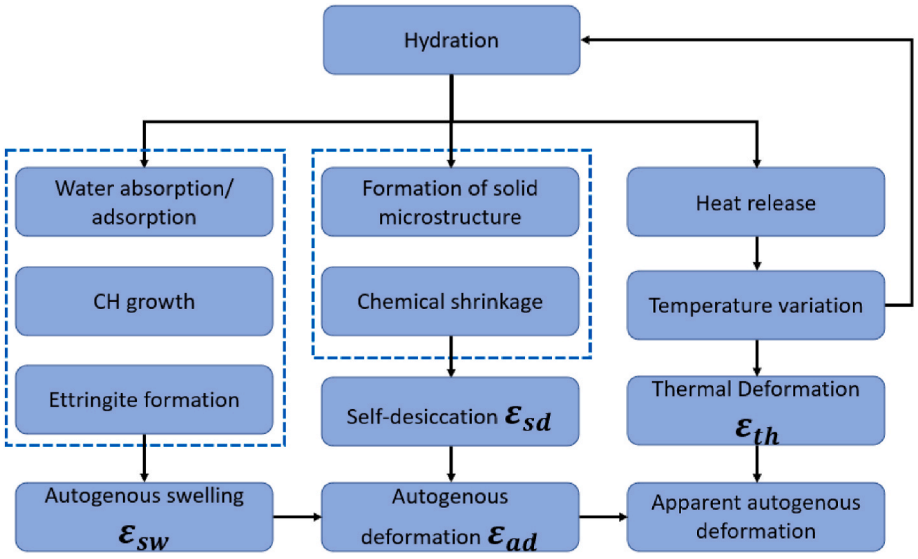

Fig. 3. Mechanisms of autogenous deformation of cementitious materials (Adapted from (Carette and Staquet, 2018)).

assembly process, the ability to commence measurements earlier, and the maintenance of high accuracy, exemplified by a resolution of 0.5 μm (Serdar et al., 2020). The moisture loss and drying shrinkage can be easily prevented with good sealing, but the effects of temperature on the AD measurement require more complex measures. If strict temperature control in the specimen is not possible, it is often necessary to separate the real AD from the total deformation by deducing the thermal deformation indirectly based on the measurement of an embedded thermo-couple (Zhang et al., 2003; Bjøntegaard and Sellevold, 2001) or other sensors such as an optical fiber (Viviani et al., 2007). However, it is important to note that even if thermal deformation can be effectively identified and separated from the total deformation using accurate coefficient of thermal expansion/contraction (CTE/CTC) (Li et al., 2021a) and temperature data, the residual effects of temperature on the hydration kinetics remain a significant factor and should not be overlooked. Therefore, active temperature control is favorable for measuring pure AD by maintaining a strict constant temperature during the test (Lura et al., 2001). Another problem with these tests is that the test can only start at least after setting when the cement paste is strong enough for displacement measurement. Therefore, such tests may neglect the initial part of AD and make the starting time of the AD measurement, referred to as time-zero, a debatable issue. Studies on the time-zero suggested different definitions, including the final setting time (Darquennes et al., 2011a), the timing of the autogenous swelling peak for slag cement concrete (Darquennes et al., 2011a), the onset of RH drop (Huang and Ye, 2017), the onset of capillary pressure (Ma et al., 2019), and transition point from the autogenous strain curve (Filho et al., 2019).

Another kind of AD test, the so-called corrugated tube test, overcomes the time-zero issue by casting the cementitious material in a plastic corrugated tube and then measures the length change from the two sides (Mejlhede Jensen and Freiesleben Hansen, 1995), as shown in Fig. 4(a). The corrugated tube is considerably stiffer in the radial than in the longitudinal direction, which enables the measurement of linear deformation by following the displacement of the corrugated tube at either end. By putting the corrugated tube in a temperature-controlled oil bath, the effects of temperature on AD measurement can be eliminated (Lu et al., 2020a). A statistical study (Wyrzykowski et al., 2017) has proven that the corrugated tube test is sufficiently sensitive to identify the AD of different levels, despite the considerably high scatter that may occur due to the inaccuracies in the initial measurement. Moreover, because the standard corrugated tube is only 22 mm in diameter (Mejlhede Jensen and Freiesleben Hansen, 1995), corrugated tube tests were initially only used on cement pastes and fine-grained mortars. By changing the size of the corrugated tube, it has been also possible to test the AD of concrete since the placement of material (Carette et al., 2018), as shown in Fig. 4(b). Despite the advantages mentioned above, the use of corrugated tube brings issues when filling and compacting the fresh material, which necessitates extra attention when casting the specimens.

Despite the convenience and accuracy of the corrugated tube test, the AD it measures cannot directly be related to the EAS, which is a more straightforward indicator of EAC. It was recently reported that the specimen geometry influences the AD measurement (Sun et al., 2022a), which poses questions about whether the corrugated-shaped specimen is representative of real-world structures. The Temperature Stress Testing Machine (TSTM), which is an important testing technique for many early-age properties and behaviors of cementitious materials, involves two specimens with identical or similar geometry—one tested under free conditions and the other under restrained conditions—enabling a direct correlation between the measured AD and EAS. The specimens are sealed and covered by molds with embedded water channels for circulating temperature-regulated water to actively control the temperature inside the specimen. The deformation is measured by embedded bars in the specimen with LVDTs. An example of such an AD test, called the Autogenous Deformation Testing Machine (ADTM), is shown in Fig. 5 (Liang et al., 2023a; Lokhorst, 2001).

Based on the testing methods described above, multiple influencing factors of AD have been investigated, mainly the effects of temperature, mix design, and the use of mitigation admixtures.

2.1.2. Temperature

AD tests are conducted under a constant temperature to exclude the influence of thermal deformation and different hydration kinetics. The results of such tests can only provide limited guidance on real-world applications where the temperature always varies. According to Klausen et al. (2020), AD tested under a realistic temperature history differs significantly from that under constant temperature. In the field of cementitious materials, the maturity concept (F. Hansen and Pedersen, 1977) has been widely used to convert the mechanical properties of specimens cured under a constant temperature to that of specimens exposed to a realistic temperature history. The assumption for the maturity concept is that temperature only influences the hydration rate, and that this influence is independent of the hydration degree. However, the mechanism of AD is more complex, which is not only related to hydration degree, but also the RH, surface tension, and production of expansive products such as calcium hydroxide and ettringite, which questions the applicability of the maturity concept in AD prediction

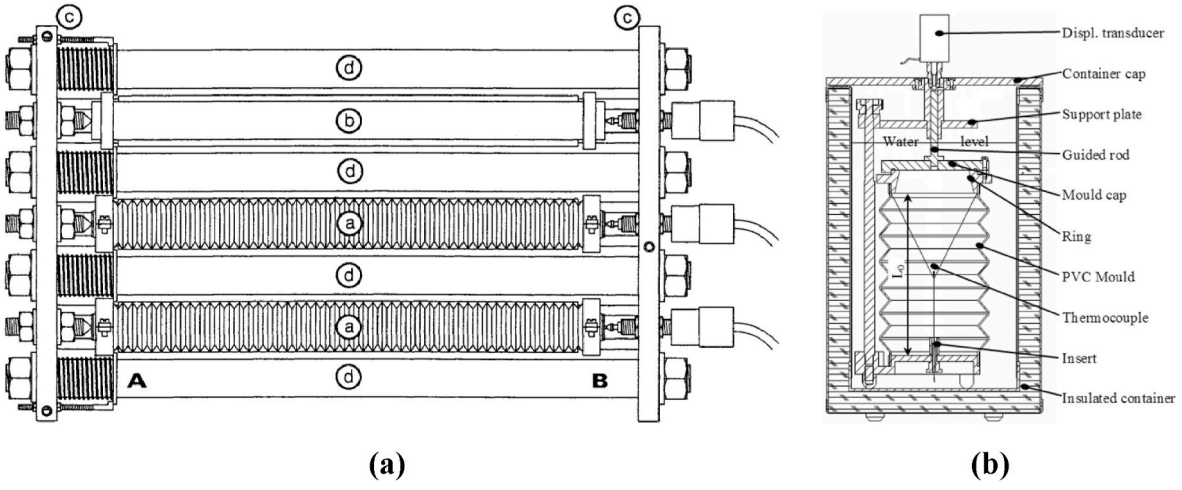

Fig. 4. Corrugated tube test: (a) standard design by (Mejlhede Jensen and Freiesleben Hansen, 1995), used mostly for cement paste and mortar (a: specimen; b: invar reference specimens; c: steel plates; d: invar rods to connect the steel plates.); (b) enlarged corrugated tube test for concrete, designed by (Carette et al., 2018).

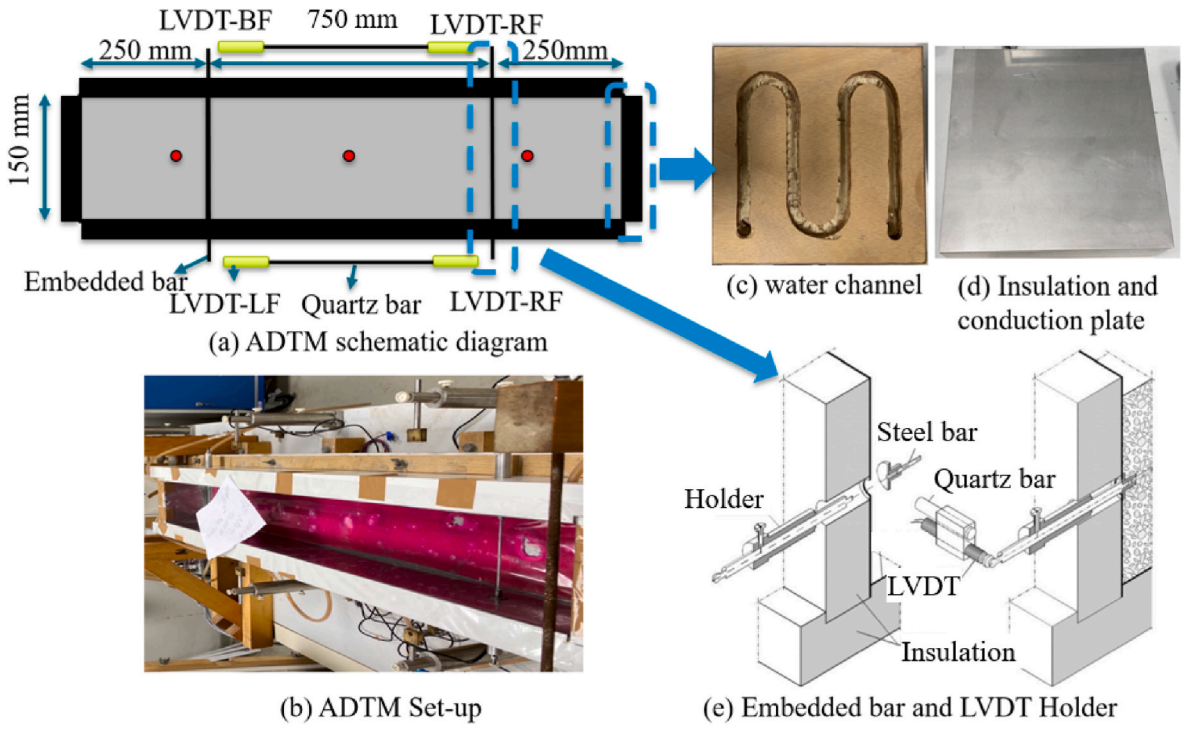

Fig. 5. AD measurement in a TSTM test (Liang et al., 2023a).

(Bjøntegaard and Sellevold, 2001; Jensen and Hansen, 1999; Jiang et al., 2014a).

The exact influence of temperature on AD is complex because temperature not only influences the RH drop and surface tension but also results in different pore structures (Reinhardt and Stegmaier, 2006). All of these parameters are related to the formation of self-desiccation shrinkage (Lura et al., 2003). Lura et al. (2001) performed AD tests based on the ADTM machine (as in Fig. 5) from 10 to 40 °C, and found that higher temperatures lead to earlier onset of shrinkage but not necessarily higher deformations. Similarly, the results of Carette et al. (Carette and Staquet, 2018) suggested an earlier onset of shrinkage when the temperature is higher. Furthermore, they also concluded that, due to the higher RH, coarser porosity, and increased solubility and decreased needle size of ettringite, the higher temperature tends to decrease the total amplitude of both autogenous swelling and self-desiccation shrinkage. However, Orosz et al. (2017) observed an opposite trend, i.e., that higher temperature leads to higher autogenous swelling, but they also mentioned the CTE may compromised their measurement. Contradictory findings regarding the influence of temperature on self-desiccation shrinkage were also found: with increasing temperature, the studies (Carette and Staquet, 2018; Loukili et al., 2000; Chu et al., 2012) observed decreased self-desiccation shrinkage while others (Li et al., 2021a; Jiang et al., 2014a; Shen et al., 2016) saw an increased one. Maruyama et al. (Maruyama and Teramoto, 2013) conducted AD tests on UHPC material and found that the influence of temperature is different before and after a so-called inflection point (i.e., when the maturity reaches 10–16 h). Before the inflection point, the AD decreases with increasing temperature and then increases afterward.

In summary, the applicability of maturity concept in predicting AD at different temperature is questionable. The increasing temperature can induce an earlier onset of self-desiccation shrinkage, which increases EAC risk. Furthermore, even with low temperatures, the rate of self-desiccation shrinkage of low-w/b ratio material is still significant, which means that EAC risk induced by AD cannot be neglected even in low-temperature environments.

2.1.3. *Mixture*

The influence of mixture design on AD can be summarized in 3 aspects, including the water-binder ratio (w/b), cementitious materials, and aggregate. The influence of w/b on AD is clear. A lower w/b ratio results in a denser pore structures and lower RH, which, according to the Kelvin-Laplace equation, can induce higher capillary pressure and therefore increase self-desiccation shrinkage. Sound experimental studies (Zhang et al., 2003; Tazawa and Miyazawa, 1995; Lee et al., 2006) verified that a lower w/b ratio induces faster self-desiccation shrinkage and therefore results in a higher EAC risk.

The influence of cementitious materials is a broad topic. An important factor is the particle size distribution of cementitious materials: the larger the particle size, the slower the RH decay and the higher the pore size. These two effects together lead to lower capillary stress and therefore a decrease of AD if cement with larger particle sizes is used (Bentz et al., 1999, 2001). Many studies also explored the influence of supplementary cementitious materials (SCMs) on AD in OPC-based blended materials. The commonly-used SCMs include Ground Granulated Blast- Furnace Slag (GGBFS), Fly Ash (FA), and Silica Fume (SF). Many researchers have observed that GGBFS (Carette et al., 2018; Lura et al., 2001; Jiang et al., 2014a; Lee et al., 2006; Bouasker et al., 2014) and SF (Zhang et al., 2003; Lu et al., 2020a; Ghafari et al., 2016) can significantly increase AD by reactive secondary hydration leading to continuous pore refinement and internal RH drop, while the use of more inert SCMs like FA (Lu et al., 2020a; Jiang et al., 2014a; Ghafari et al., 2016) and calcined dredging sediments (Van Bunderen et al., 2019) decreases AD by slowing down the hydration process. Other cementitious materials like UHPC (Zhang et al., 2019a; Ghafari et al., 2016) and limestone calcined clay cement (LC3) (Nguyen et al., 2022) were also reported to have significant AD. In addition, alkali-activated materials, which aim to replace all OPC with industrial byproducts like GGBFS, FA, metakaolin, etc., have been found to display a more significant AD development that is often multiple times higher than OPC-based concretes, due to the more rapid hydration kinetics and a much denser pore structure (Li et al., 2019a, 2020a).

The influence of aggregate on AD can be summarized in 3 effects, including effects of dilution, restraint, and internal curing. The use of

aggregates reduces the volume ratio of cementitious materials and directly reduces development of AD in concrete (Liu and Hansen, 2016). Furthermore, natural dense aggregates act as internal restraint in the cement matrix and lead to decreased AD (Lu et al., 2021). As shown in Fig. 6, such restraining effects can result in a heterogeneous strain field and can be visualized by digital image correlation (DIC) to investigate the exact influence of aggregate size and distribution (Chen et al., 2018; Gao et al., 2021). On the other hand, saturated porous aggregate (e.g., lightweight aggregate, recycled concrete aggregate, etc.) acts as an internal water reservoir which gradually releases water and slows down the RH drop, alleviates the self-desiccation process, and thereby decreases the AD (Mao et al., 2021; Zhutovsky et al., 2002; Bentur et al., 2001). However, it is crucial to acknowledge that incorporating porous aggregates can adversely affect the mechanical properties of the concrete. Therefore, a careful optimization process is essential, taking into account not only the type and volume of aggregate used but also its shape, to effectively reduce AD while maintaining the necessary mechanical performance of the material (Akcay and Tasdemir, 2009; Zhuang et al., 2016).

2.1.4. Mitigation strategies

Most mitigation strategies for AD prevention are based on the following mechanisms: control of hydration, reduction of surface tension of the pore solution, the addition of internal restraint, formation of expansive products, and internal curing (Yang et al., 2019).

For control of hydration, the use of SCMs is a common measure, as discussed in section 2.1.4. In addition, superplasticizers and viscosity-modifying agents that delay the hydration reaction can also decrease AD (Tazawa and Miyazawa, 1995; Valcuende et al., 2012). Shrinkage-reducing agents (SRA) decrease the surface tension of the pore solution to reduce the capillary pressure which leads to reduction of AD (Zhang et al., 2022a,b,c; Klausen and Kanstad, 2021; Zhan and He, 2019; Moelich et al., 2022). Recently, Zhang et al. (2022d) developed a shrinkage-reducing polycarboxylate superplasticizer which substantially reduces AD by combining the effects of delayed hydration, reduced surface tension, and formation of expansive products (i.e., portlandite). Internal restraint can often be achieved by aggregate (as in Section 2.1.4), reinforcement (Zhao et al., 2022), and various types of fibers (e.g., steel fiber (Zhang et al., 2019a), cellulose fiber (Feng et al., 2022), Barchip fiber (Shen et al., 2020a) etc.). The formation of expansive products by calcium sulfoaluminate cement (Sirtoli et al., 2019, 2020) or CaO-based expansive agent (Zhao et al., 2021, 2022) was proven to effectively compensate the self-desiccation shrinkage by producing expansive products like ettringite and portlandite. Internal curing by either lightweight aggregate or superabsorbent polymers (SAP) is a straightforward countermeasure against self-desiccation and has been proven by many studies as a very effective solution (Bentur et al., 2001; Justs et al., 2015). The use of lightweight aggregate has been introduced in Section 2.1.4. Despite having a negative influence on the mechanical properties, it was observed that the pre-wetted SAP partially fills with portlandite during cement hydration, delays the main hydration peak, and increases the hydration degree after a few days (Justs et al., 2015). The success of SAP was also observed in FA and GGBFS- blended binders and LC3 pastes (Snoeck et al., 2015; Chen et al., 2023).

2.2. Sub model 1: modelling the autogenous deformation

There are two categories of models for predicting AD: empirical models and theoretical/physical models. The empirical models are the results of statistical analysis of experimental data and are commonly used by researchers and engineers due to their convenience. The theoretical/physical models aim to predict the AD by simulating the underlying mechanisms.

2.2.1. Empirical models

Most formula-based empirical models assume that AD is the product of two components, an ultimate AD $\varepsilon_{au,e}$, and a time-decaying function f (mostly power function), as below.

$$\varepsilon_{au} = \varepsilon_{aue}(mix, env) \times f(t, mix, env) \tag{1}$$

where the $\boldsymbol{\varepsilon_{aue}}$ and f are both dependent mainly on the mixture and environmental parameters. The form of an empirical model as described by Eq. (1) is widely adopted by different design codes (Lai et al., 2021; Hubler et al., 2015a; Sakata and Shimomura, 2004; Raphael et al., 2012). As the autogenous swelling is seldom mentioned even in tests, the code-based formulas assume AD a monotonically-decaying function as given by Eq. (1). Contrarily, based on the corrugated tube test for concrete (Fig. 4(b)), Carette and Staquet (2018), Carette et al. (2018) built a semi-empirical model that considers AD as a sum of autogenous swelling and self-desiccation shrinkage, which is induced by ettringite formation and capillary pressure respectively.

Another kind of empirical model was constructed based on Machine Learning (ML) algorithms like Extreme Gradient Boosting or Artificial Neural Network, which showed significantly better performance than traditional empirical models (Hilloulin and Tran, 2022; Bal and Buyle-Bodin, 2013). The ML approach train sophisticated ML models with massive data to obtain generalizing capabilities for predictions of

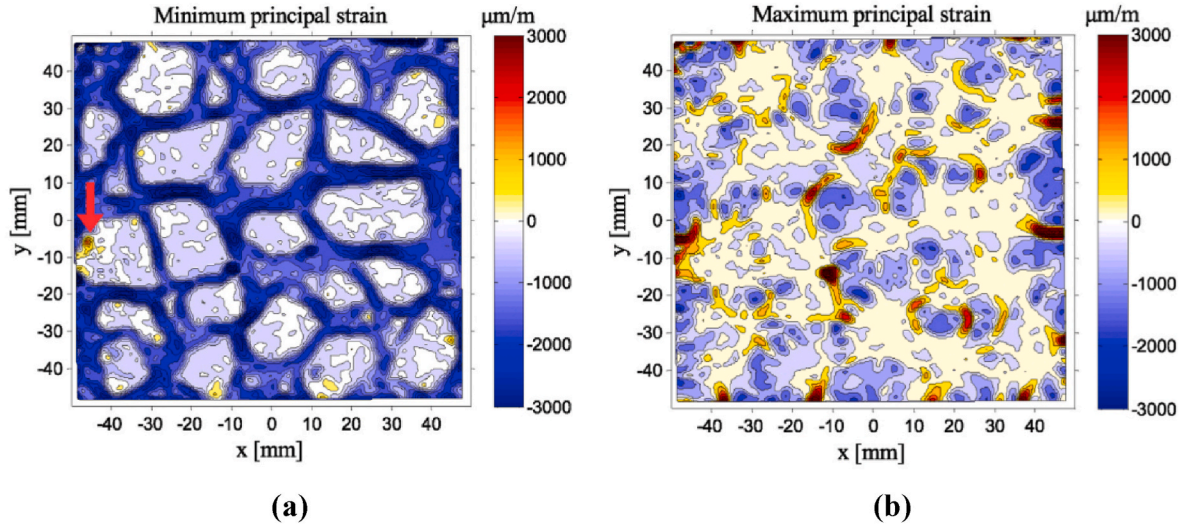

Fig. 6. Drying shrinkage captured by DIC, adapted from (Gao et al., 2021): (a) minimum principal strains; (b) maximum principal strains.

AD in different scenarios and may be a promising approach to replace the formula-based empirical models.

2.2.2. Theoretical models

Theoretical models aim to predict the AD from the underlying mechanisms at different physical fields, as shown in Fig. 7. Constructing such a model including all (or most) relevant mechanisms involves a multiscale and multi-fields analysis, typically with a hygro-field for moisture transport, chemo-field for hydration reaction, thermo-field for heat transport, and mechanical field for deformation calculation. Such multi-field model is still a challenge due to its complexity. However, some studies managed to build such unified models. Pichler et al. (2007) employed a kinetic law (Bernard et al., 2003) to simulate the hydration reaction of cement with different chemical constituents and obtain the overall hydration kinetics and microstructural parameters (products by volume percentage). Assuming capillary pressure (induced by self-desiccation) and crystal pressure (induced by ettringite formation) as the main driving force of AD, they applied micromechanics to calculate the elastic deformation of a homogenized composite as the AD, by homogenizing the elastic modulus of different phases from the scale of Calcium-Silicate-Hydrate (C–S–H) to concrete. Pathirage et al. (2019) used the Cement Hydration in Three Dimensions (CEMHYD3D) model at the microscale to obtain the material properties as input for a Hygro-Themo-Chemo (HTC) model (Di Luzio and Cusatis, 2009a,b) at the macroscale to simulate the RH drop (i.e., self-desiccation). Zhao et al. (2019a) used the Hymostruc model (Koenders and van Breugel, 1997; van Breugel, 1995; Ye et al., 2003) for calculating the RH drop and Shimomura model (Shimomura and Maekawa, 1997) for calculating the pore size distribution. Based on the micromechanics, the homogenized elastic properties of concrete were obtained by an upscaling process from C–S–H to concrete, and the AD was calculated as the elastic response to the capillary pressure.

While the models mentioned above have already encompassed a combination of complex mechanisms, room for improvements still exist. Specifically, while the model in Pathirage et al. (2019) did not extend further to mechanical field to predict the AD, the models in Pichler et al. (2007), Zhao et al. (2019a) only assumed AD as the elastic response of the microstructure to the capillary pressure, which is problematic because the early-age cementitious material is at least a viscoelastic material (if neglecting visco-elasto-plasticity at high stress condition). Based on the capillary pressure theory and micro-poromechanics, Aili et al. (2018) concluded that the long-term AD evolves logarithmically and that AD is a viscoelastic response to self-desiccation. In view of the necessity of considering creep in AD prediction, Gao et al. (2022) used the Hymostruc model (Koenders and van Breugel, 1997; van Breugel, 1995; Ye et al., 2003) to obtain the microstructure and the RH drop. Based on the obtained microstructure, they built the lattice fracture model (Schlangen and Garboczi, 1997) and applied internal loads (calculated by the capillary pressure) on the lattice beams to simulate the compression of the microstructure induced by self-desiccation. The creep effects were considered by using a penalized effective modulus, which was determined by calculating the compression creep of a simple one-dimensional loaded beam.

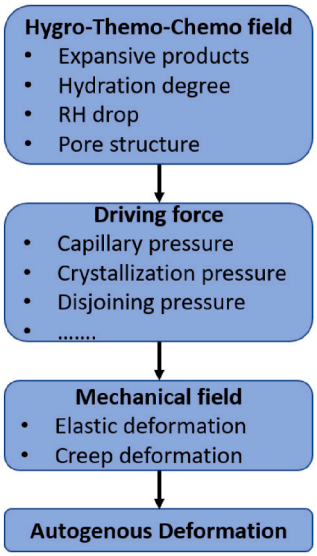

Fig. 7. Underlying mechanisms for theoretical models of AD prediction.

Other models focused more on the quantification of the driving force (i.e., capillary pressure in most cases) and mechanical field, left out the HTC field, and used experimental data or other empirical models for the input of pore size distribution, RH drop, heat release, etc. Huang et al. (2020) used a series of empirical models for the input of RH, hydration degree, saturation degree, elastic modulus, etc., and then calculated AD as the elastic response to the capillary pressure. Hu et al. (2019a) used a Kelvin-Voigt model to simulate the aging viscoelasticity of cement pastes and calculated the self-desiccation shrinkage based on poro-mechanics, using the experimental data of RH, elastic modulus, and creep as input. Lu et al. (2020b) considered the AD as the combination of the elastic part and the creep part and calculated the AD by a linear superposition of incremental viscoelastic deformation based on the internal capillary pressure theory. The early-age creep was obtained from the activation energy concept (Klug and Wittmann, 1974). Furthermore, the Pickett Effect was incorporated to simulate the restraining effect of aggregate (Lu et al., 2021), which not only resulted in a good prediction for Portland cement concrete but also for alkali-activated slag and fly ash concrete (Li et al., 2021b).

The models for AD prediction are summarized and compared in Table 1. All models considered capillary pressure as the driving force behind self-desiccation shrinkage. This is valid for early-age material because the capillary pressure is the main driving force for RH above 40–50%, while other mechanisms, including disjoining pressure, surface tension, and interlayer water, mostly occur at RH lower than 40%, which is generally not the case for early-age materials (Tang et al., 2021). By comparison, it seems that the model in Gao et al. (2022), i.e., a combination of Hymostruc and Lattice Fracture Model, is until now the most complete model that encompasses the hydration reaction, self-desiccation, and the viscoelastic response to the capillary pressure from the microscale. It should still be noted that the model of Gao et al. (2022) and many other models except for Pichler et al. (2007) only considered the self-desiccation shrinkage as AD and considered the capillary pressure as the driving force. This is understandable since the self-desiccation shrinkage is indeed the most relevant risk factor regarding EAC. However, the contribution of autogenous swelling should not be neglected, otherwise the EAS calculated based on the AD will be overly conservative. Another concern is that the constitutive model of the mechanical field in Gao et al. (2022) only considered the creep effects by effective modules, while the superposition of incremental creep strain was done with a simple one-dimensional beam, which did not take account of the real strain history in the elements. Finally, one more thing worth being noted is that only the model of Pathirage et al. (2019) explicitly simulated the hygro-field for RH drop in self-desiccation, while the others only calculated the RH drop indirectly. However, their model (Pathirage et al., 2019) focused only on the self-desiccation and RH drop, and did not extend to the mechanical field to predict the AD.

3. Viscoelastic properties

Viscoelastic properties determine the rate of EAS buildup per restrained AD, which can be quantified by two kinds of parameters: elastic modulus for elasticity and creep compliance or relaxation modulus for viscosity. In a loading test, elastic modulus can be calculated as the slope of the stress-strain curve of the load-increasing or

Table 1
Summary of analytical models for AD prediction.

Ref.	Pore	RH	Elastic Modulus	Creep	Driving force	Mechanical model
Pichler et al. (2007)	Kinetics law and others		Micromechanics	–	Capillary and crystallization pressure	Micromechanics
Pathirage et al. (2019)	CEMHYD3D and HTC model		–	–	–	–
Huang et al. (2020)	Empirical formula			–	Capillary pressure	Poromechanics
Zhao et al. (2019a)	Shimomura model	HymoStruc model	Micromechanics	–	Capillary pressure	Micromechanics
Aili et al. (2018)	Empirical formula		Micromechanics with non-aging properties		Capillary pressure	Micro-poromechanics
Gao et al. (2022)	HymoStruc		Properties of each micro phase (obtained from literatures)		Capillary pressure	Lattice Fracture Model with effective modulus for creep effects
Hu et al. (2019a)	Test	Test	Test	Test	Capillary pressure	Poromechanics
Lu et al. (2020b, 2021)	Test	Test	Test	Activation energy concept	Capillary pressure	Poromechanics with Pickett effect

-decreasing part. Creep compliance refers to the strain elapsed with time induced by a constant unit load, while the relaxation modulus refers to the stress elapsed with time induced by an imposed constant unit strain (Bažant and Jirásek, 2018). Due to the technical difficulties of sustaining a constant strain in relaxation tests, creep tests are mostly conducted and used to quantify the viscosity with creep compliance (Bazant and Wu, 1974). Specifications for tests of elastic modulus and creep and their empirical formulas can be found in various designing codes for concrete structures and materials (American Concrete Institute, 2008; Hubler et al., 2015a; fib, 2013; American Concrete Institute Committee 209 (ACI), 1992; Brussels, 1986; EN, 2002; AASHTO, 2012). In the following sections, the focus is on the mechanisms, testing methods, and modelling schemes for quantifying the viscoelastic properties.

3.1. Elastic modulus

3.1.1. Macroscale tests for elastic modulus

Elastic modulus is positively correlated to the compressive strength, as revealed by macroscale loading-unloading tests (Rashid et al., 2002), and empirical formulas were well established to infer the elastic modulus from either mixture parameters or compressive strength data (fib, 2013; Zhou et al., 1995). Therefore, the influence of mixture parameters and environmental conditions on elastic modulus is generally similar to that on strength (Neville, 2011). Specifically, regarding the influence of temperature, the maturity concept was also successfully applied to predict the evolution of elastic modulus (Geng et al., 2021; Waller et al., 2004). Nevertheless, it is worth noting that the influence of aggregate on elastic modulus is more significant than that on strength (Zhou et al., 1995; Beushausen and Dittmer, 2015). The aggregate stiffness positively influences the elastic modulus of concrete, evidenced by the testing results (Zhou et al., 1995; Beushausen and Dittmer, 2015) and micromechanical analysis (da Silva et al., 2013). Moreover, despite the good accuracy of empirical formulas in prediction of elastic modulus, they are mostly calibrated for mature concrete, which casts doubts on predictions on early-age elastic modulus. The early-age elastic modulus is difficult to test by traditional loading-unloading methods because of the large number of tests needed for obtaining the elastic modulus at different ages and the challenges of preparing very soft specimens for loading test at young ages. One way to circumvent this difficulty is though in-situ testing. Boulay et al. (2014) devised a test rig called BTJASPE (French acronym for BeTon au Jeune Age, mesure de la Deformation Endogene) to monitor the development of elastic modulus immediately after casting by continuously applying compression load. The BTJASPE setup uses LVDTs to measure the strain and the mold uses temperature-regulated water to control the sample temperature. TSTM is also suitable for this test; furthermore, it allows testing of the elastic modulus under tension since most TSTM specimens are dog-bone. However, much larger specimens are needed for TSTM testing. Another novel method allowing for the continuous measurement of elastic modulus since casting time is the ambient response method. Following such method, the elastic modulus of the hardening cementitious materials can be calculated based on modal identification of a composite beam (Serdar et al., 2020). Elastic modulus at early ages can also be measured indirectly, e.g., by the ultrasonic pulse velocity (UPV) (Carette and Staquet, 2016).

3.1.2. Microscale tests and micromechanical modelling for elastic modulus

The microscale tests of elastic modulus aim for a more fundamental understanding and lays foundations for a reliable prediction model. OPC paste can be seen as a composite of various hydration products, including phases like C–S–H, calcium hydrate, unhydrated particles, etc. (Constantinides and Ulm, 2004; Tennis and Jennings, 2000). Assuming the distribution of the mechanical properties of each kind of hydration product is a Gaussian distribution, statistical nanoindentation tests have often been used to extract the average mechanical properties of each phase in hydrated cement paste, allowing for the effective mechanical properties of the composite to be calculated based on a micromechanical model using the averaged modulus and volume fraction of each phase as input (Constantinides and Ulm, 2004; Sorelli et al., 2008; Da Silva et al., 2014; Li et al., 2019b). Except for Gaussian-based method, other methods like K-Means Clustering (Chen et al., 2021) can also be used for the deconvolution process. The real effective elastic modulus is often obtained by microindentation test (Hu et al., 2020a) to validate the results of micromechanical models. Such methods have been successfully used to predict the effective elastic modulus of different cementitious materials, including blended cement pastes (Wilson et al., 2018), polymer-modified cement pastes (Göbel et al., 2018), geopolymers (Fang et al., 2021; Luo et al., 2021), seawater-mixed alite pastes (Sun et al., 2022b), and nature pozzolan concrete (Wilson et al., 2017). However, note that except for the micromechanical model, Lattice Fracture Model (Šavija et al., 2020; Zhang et al., 2017, 2019b, 2020) and other FEM models (Lee and Park, 2008) are also able to do the upscaling from several phases to the effective properties of the composite. Once the homogenization scheme (either by micromechanics, Lattice Fracture Model, or other FEM methods) is settled and validated by nano- and micro-indentation, the time-dependent elastic modulus can be obtained by using a hydration model which provides evolution of volume fractions of each micro phases, as in Bernard et al. (2003), Krishnya et al. (2021), Princigallo et al. (2003), Šmilauer and Bittnar (2006). Despite that these models showed satisfactory accuracy in different cases, difficulties still exist with the quantification of interfacial transition zone (ITZ) properties, which was considered in Li et al. (20199b), Lee and Park (2008), Liang et al. (2017).

3.2. Creep/relaxation

The viscoelastic properties can be quantified by both creep compliance and relaxation modulus. With a linear viscoelastic constitutive relationship, following the Boltzmann superposition, the strain history induced by a varying stress history can be calculated as:

$$\varepsilon(t_f) = J(t_0, t_f)\sigma(t_0) + \int_{t_{0+}}^{t_f} J(t', t_f)\dot{\sigma}(t')dt' \quad (2)$$

where the ε is the strain; σ is the stress; J is the creep compliance function; t_0 is the time when the load is first applied; t_f is the time step of interest; The dot (·) notation above a variable is the operation of taking the derivative with respect to time. Then, considering the boundary of a relaxation test (i.e., $\varepsilon(t_f) = 1$) and definition of relaxation modulus, Eq. (2) leads to:

$$1 = J(t_0, t_f)R(t_0, t_0) + \int_{t_{0+}}^{t_f} J(t', t_f)\dot{R}(t_0, t')dt' \quad (3)$$

where R is the relaxation modulus. Eq. (3) means that the creep compliance and the relaxation modulus are not independent from each other. Despite being obtained from mechanical tests with different boundary conditions, creep compliance and relaxation modulus are equivalent representation for the viscoelastic properties of the material (Bažant and Jirásek, 2018).

3.2.1. Experiments for creep/relaxation

Measuring the relaxation modulus is much more challenging than testing the creep compliance, because the relaxation test needs not only the strain measurement but also a loading system that actively adjusts the load to maintain the constant strain, which is the principle behind the TSTM test. For the creep test, one only needs to keep the load constant and measure the strain, which is more straightforward and therefore is adopted by most studies.

3.2.1.1. Macroscale testing. Macroscale testing directly provides input for the EAS simulation. While studies have been devoted to long-term creep (Charpin et al., 2018), the main interest of EAC analysis is the early-age creep, which requires multiple creep measurements during early stages of hydration. In other words, the specimen needs to be loaded multiple times to obtain the creep at different ages. However, at early age during the load-holding stage, which can last from hours to days, when the creep deformation is happening, the properties of the hardening specimen also evolve very fast. As a result, the measured deformation during the load-holding stage is a combined effect of creep and hydration. In view of this, hourly repeated minute-long quasi-static tests for creep have been proposed (Irfan-ul-Hassan et al., 2016; Delsaute et al., 2016; Ausweger et al., 2019; Huang et al., 2019; Delsaute et al., 2017). The main advantage of this test is that, with a load-holding stage of only 3 min, the hydration effects can be neglected, and the deformation tested then represents well the creep strain obtained at corresponding loading age. Moreover, such a test allows for creep measurement in every hour, and obtains the elastic modulus in every loading-unloading process. Therefore, the hourly repeated minute-long quasi-static test alone is already able to provide the input of viscoelastic properties for EAS simulation. Another test that aims to exclude the effect of hydration on creep measurement is the so-called equivalent systems test (Wyrzykowski et al., 2019), where part of the unhydrated cement is replaced with inert filler to emulate specific microstructural features of the real hydrating systems. However, as their results showed, the real systems experienced much higher creep than the equivalent inert systems.

There are also other improved macroscale creep tests. By assuming that the drying shrinkage is symmetric about the neutral plain and does not influence the deflection, the four-point bending test was proposed to measure the creep properties, which is reflected by the deflection measurement (Liang and Wei, 2019; Wei et al., 2020; Farah et al., 2019). The TSTM-based creep test allows for measurement of compressive and tensile creep with specified temperature history, thanks to the capacity of the designed setup (Dabarera et al., 2021). Another kind of TSTM-based creep test, i.e., a double feedback control test (Zhu et al., 2018), was proposed to test the creep deformation under restraint condition. Such test was specified to restraint test controlled by a threshold value of the deformation. In each testing increment, two feedback loops were implemented, including the control of the deformation by a threshold value and the control of the load at a constant value. The total creep deformation was then the sum of the measured creep in all testing cycles. Furthermore, the creep strain measurement can also be combined with other more advanced monitoring techniques, such as acoustic emission measurement (Li et al., 2021c) to quantify the influence of damage degree on the creep measurement. Macroscale creep tests investigated many influencing factors. In blended cement systems, it was found that the use of FA, quarts, and glass powder significantly increases creep (Zhao et al., 2019b; Hu et al., 2020b; He et al., 2019), while the use of GGBFS may decrease creep and the influence of GGBFS compositions was highlighted (Gu et al., 2019; Delsaute et al., 2021). In addition, the effects of other parameters on creep, such as temperature (Briffaut et al., 2012), w/c ratio (Shen et al., 2017), lightweight aggregate (Zheng et al., 2019), recycled concrete aggregate (Silva et al., 2015), steel fiber (Zheng et al., 2019; Zhu et al., 2020a), MgO (Zhao et al., 2020), and SAP (Li et al., 2022a) were also extensively investigated by macroscale tests.

The influence of temperature on creep was mainly by two different mechanisms (Bažant et al., 2004): 1) A temperature increase accelerates the bond breakages and restorations causing creep, and thus increases the creep rate as seen by studies (Briffaut et al., 2012; Liang et al., 2022c); 2) A temperature increase accelerates the hydration and therefore reduces the creep. For early-age concrete, the effects of hydration dominates and therefore the maturity concept can still be used for predicting the basic creep at the early age (Bažant et al., 2004; De Schutter, 2004). The increase of RH can increase the long-term creep rate (Liang et al., 2022c; Frech-Baronet et al., 2017), and can be quantified by the microprestress-solidification theory (Bažant et al., 2004; Yu et al., 2020). For EAS analysis, the influence of compressive or tensile creep is important, because EAS typically initiates with compressive stress resulting from expansion, subsequently transitioning to tensile stress as shrinkage happens. However, a consensus regarding the influence of creep in tension and compression has not been reached yet. The testing results of Atrushi (2003) suggested that creep in tension is lower initially but establishes a much higher rate than in compression. Similarly, Rossi et al. (2013) observed that compressive creep is more significant than tensile creep, but they also saw that compressive and tensile creep are similar under drying conditions. By contrast, many other studies suggested that compressive and tensile creep are similar, and that it is justifiable to use compressive creep to substitute tensile creep (Bažant and Jirásek, 2018; Briffaut et al., 2012; Klausen et al., 2017; Wei et al., 2018).

3.2.1.2. Micro-scale testing. Micro-scale creep tests aim to reveal more fundamental mechanisms of creep behavior and lay foundation of micromechanical prediction models for predicting creep properties. Minutes-long micro- or nano-indentation tests are widely used for obtaining the creep properties of cementitious materials at the microscale (Hu et al., 2020a; Frech-Baronet et al., 2017; Zhang et al., 2014; Wei et al., 2017a; Mallick et al., 2019a,b; Liang and Wei, 2020a,b; Li et al., 2021d). One major advantage of such test is that it can efficiently also quantify the long-term creep properties, which is significantly faster than macroscale tests (Vandamme and Ulm, 2013). In addition,

micro-cantilever tests have also been used to characterize the creep properties at microscale (Gan et al., 2020). Microscale tests offered fundamental understandings on creep mechanisms. Hu et al. (2020a) identified the influence of Ca/Si ratio on creep modulus and quantified that the creep modulus of CSH is 180 GPa. Liang et al. (Liang and Wei, 2020a) found that the long-term creep rate of cement paste appeared to be independent of loading duration, holding duration, indentation force amplitude, and unloading duration of the microindentation tests, suggesting it is an intrinsic material parameter. Li et al. (2021d) observed that the deviatoric stress-induced preferred orientation of crystallites significantly influence the creep behavior. The influence of other parameters on the creep mechanisms of cementitious materials at the microscale was also extensively investigated by microindentation tests, such as the effects of capillary water (Mallick et al., 2019a,b), relative humidity (Suwanmaneechot et al., 2020), initial viscosity (Liang and Wei, 2020b), and porosity (Li et al., 2022b).

3.2.2. Sub model 2: modelling the viscoelastic properties

Models for creep predictions includes two categories, empirical models and analytical/numerical models. The empirical models are often the statistical results of massive data of macroscale tests, while the analytical models are from the perspective of micromechanics.

3.2.2.1. Empirical models. In empirical models, creep compliance function is usually expressed in the following form

$$J(t_0,t)=\frac{1}{E(t_0)}+C_0C_1(t_0)C_2(t-t_0) \tag{4}$$

where the E is the elastic modulus; t_0 is the time when load was applied; t is the time of interest; t-t_0 is the time elapsed since the load is applied; C_0 is a fitting parameter related to mixture and environment; C_1 is the function of t_0, which describes the aging of creep compliance, and should also be dependent on mixture and environment; C_2 is the function of t-t_0, which describes the non-aging creep, and should also be dependent on mixture and environment. Many design codes (American Concrete Institute, 2008; Hubler et al., 2015a; fib, 2013; American Concrete Institute Committee 209 (ACI), 1992; Brussels, 1986; EN, 2002; AASHTO, 2012) adopted Eq. (4) as the form of their fitting formula of creep compliance. A major difference between different codes may be the choice of the non-aging function C_2, which is often a power function for description of short-term creep (Gan et al., 2020; Bazant and Osman, 1976) and a logarithmic function for long-term creep (Charpin et al., 2018; Zhang et al., 2014; Mallick et al., 2019b; Vandamme and Ulm, 2013; Torrenti and Le Roy, 2018). Besides, improvements to the empirical formulas have been achieved by incorporating other representative parameters, such as the fictitious degree of hydration (De Schutter and Taerwe, 2000; Jiang et al., 2014b), age-adjusted effective modulus (Wang and Gong, 2019), and hydration degree of slag (Delsaute et al., 2021).

Another form of empirical models are the ML-based models, such as Artificial Neural Network (Bal and Buyle-Bodin, 2014), Genetic Programming (Gandomi et al., 2016), Support Vector Machine (Li et al., 2021e), ensemble model (Liang et al., 2022c), and Deep Convolutional Neural Networks (Liang et al., 2022d). These models were mostly trained on massive database of creep tests (Bažant and Li, 2008; Hubler et al., 2015b), and show superior prediction accuracy compared to traditional codes on predicting the creep behavior of cementitious materials.

3.2.2.2. Theoretical models. Before discussing the analytical models for creep, it is important to note that for EAS analysis, the input of creep compliance needs to be a fast-aging function. An important theory to describe the aging of creep is the solidification theory (Carol and Bažant, 1993; Hedegaard, 2020; Zdenek Bazant et al.), which considers aging as resulting from the progressive solidification of a basic constituent that behaves as a non-aging viscoelastic material. Based on the solidification theory, the Microprestress-Solidification theory (Bažant and Jirásek, 2018; Zhao et al., 2020; Yu et al., 2020) was developed and constantly improved to describe the influence of temperature and RH. For description of the non-aging term of creep, rheological models including Kelvin Chain and Maxwell chain (Hu et al., 2020b; Briffaut et al., 2012; Zhao et al., 2020; Hilaire et al., 2013; Hedegaard et al., 2015) can be used, by fitting the governing equation of the rheological model with the experimental data. To describe aging, a spectrum of rheological chains is needed, which can often be calculated with the continuous retardation chain method (Bažant and Xi, 1995; Jirásek and Havlásek, 2014; Bazant et al., 1995). Then, rheological models can be used in a Finite Element Model (FEM) to calculate the creep behavior of concrete structures, using the rate-type form and exponential algorithm (Bažant and Jirásek, 2018; Bazant and Wu, 1974; Yu et al., 2012; Di Luzio et al., 2020).

Similar to the modelling methods of elastic modulus in Section 3.1.2, based on the microscale and macroscale tests, multiscale models were built to describe the overall creep behavior of a multiphase composite based on the input of the build-block phases, such as CSH, CH, unhydrated particles at microscale and aggregate, ITZ at mesoscale. In such multiscale models (Honorio et al., 2016; Li et al., 2021f), the creep compliance is often quantified as creep modulus and the input of each single phase needs to be obtained from nanoindentation tests. Based on a quasi-elastic relationship between creep and relaxation in the Carson-Laplace space (Vandamme and Ulm, 2013; Aili et al., 2020), the elastic micromechanical homogenization schemes such as Mori-Tanaka scheme (Mori and Tanaka, 1973) or the Self-Consistent scheme (Hill, 1965) can be used to calculate the effective creep modulus from a composite of phases with different creep modulus and volume fractions. Königsberger et al. (2021) compared the results of three micromechanical models with macroscopic samples of cement paste, mortar, and concrete, and demonstrated the feasibility of such upscaling method by micromechanical models. Baronet et al. (2022) proposed a two-scale micromechanical model to characterize the logarithmic creep of concrete by coupling the microindentation and uniaxial compression creep test. Except for the micromechanical model, other FEM models (Hu et al., 2019b) and Lattice Fracture Models (Gan et al., 2021) can also be used for such upscaling. Following the solidification theory, that aging of creep is the progressive volume change of hydration products and unhydrated particles, the aging creep can be obtained by coupling the micromechanical models and a hydration model, as done by Lavergne et al. (Lavergne and Barthélémy, 2020).

For analysis of EAS, the time-dependent viscoelastic properties (i.e., aging creep and elastic modulus) are important input. The multiscale modelling schemes for creep and elastic modulus are similar, as introduced in Section 3.1.2. A general description of such multiscale modelling scheme is shown in Fig. 8. For elastic modulus, a direct implementation of the elastic micromechanical homogenization schemes (like in Constantinides and Ulm (2004), Sorelli et al. (2008), Da Silva et al. (2014), Li et al. (2019b)), or a simulation of a loading-unloading test by a lattice model (or other FEMs, like in Šavija et al. (2020), Zhang et al. (2019b), Zhang et al. (2017), Zhang et al. (2020), Lee and Park (2008)) is sufficient. For creep modulus, the elastic micromechanics needs to be implemented in Carson-Laplace space (like in Honorio et al. (2016), Li et al. (2021f)), in which the relaxation and creep follow a quasi-elastic constitutive relationship. If using Lattice model or other FEMs for creep modulus (like in Hu et al. (2019b), Gan et al. (2021)), the input of creep of each phase needs to be discretized into rheological chains, and then the integral of creep needs to be calculated by either direct integration or by a more efficient algorithm, like the exponential algorithm.

4. Early-age stress

EAS is the combined result of restrained AD and aging viscoelastic properties of concrete. Considering the heterogeneity of concrete, in-

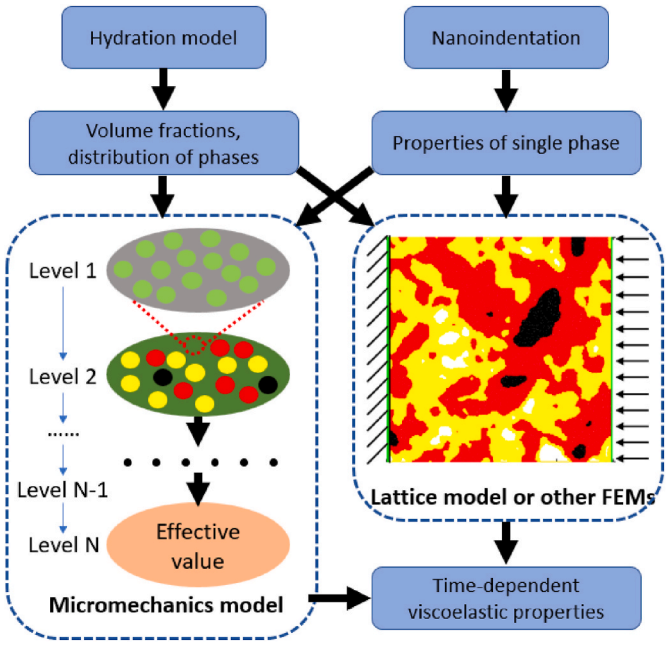

Fig. 8. General procedure of multiscale modelling for viscoelastic properties of cementitious materials.

ternal restraint formed by aggregate can also induce stress, which is often referred to as "eigen-stress". As a concept at the micro- or meso-scale, the eigen-stress can influence the mechanical properties such as strength and stiffness (Awasthy et al., 2023). In this paper, the EAS modelling is mainly on macroscale and is induced by external restraint. Understanding and quantifying EAS is a significant step to further analyze the EAC risk. Intrinsically, EAS is the result of a relaxation test, which aims to measure the stress evolution under a series of imposed deformation (i.e., restrained AD that happens constantly during the hydration of restrained concrete). Such relaxation test can be described by the following integral,

$$\sigma(t) = \int_0^t R(t_0, t)\dot{\varepsilon}(t_0)\mathrm{d}t_0 \tag{5}$$

where R (t_0, t) is the relaxation modulus; $\varepsilon(t_0)$ is the imposed deformation; $(\cdot)$ is the derivative with respect to time. Eq. (5) clearly illustrates that if the aging viscoelastic properties R (t_0, t) and the AD $\varepsilon(t_0)$ are known, the EAS can be directly calculated. However, the complexity lies in the quantification of R (t_0, t) and $\varepsilon(t_0)$, either experimentally or numerically based on the approaches described in Sections 2 And 3.

4.1. Experiment

The EAS can be tested by well-designed passive or active restrained tests (Serdar et al., 2020), such as the internal restraint test (Semianiuk et al., 2017; Lura et al., 2009), rigid cracking frame test (Spingenschmid, 1998), ring test (Briffaut et al., 2016; Gao et al., 2013; Shen et al., 2019, 2020b), and temperature stress testing machine (TSTM) (Shen et al., 2016; Klausen et al., 2019). Among these tests, a TSTM system appears to be the most versatile because it can not only measure the EAS, but also AD and creep if given a different boundary condition (Xin et al., 2020; Klausen, 2016). Moreover, a TSTM system includes strict temperature control to simulate various realistic thermal conditions. A TSTM system alone encompasses all required input and output of Eq. (5), and thus provide a solid basis of a more thorough understanding and a reliable prediction model for EAS. This section will then focus on the TSTM.

4.1.1. TSTMs

The general design of a TSTM system, which is broadly adopted by most TSTM studies such as Nguyen et al. (2019), Klausen (2016), Lokhorst (2001), Shen et al. (2016), Springenschmid et al. (1994), Igarashi et al. (2000), Bjøntegaard (1999), Ou et al. (2023), is shown in Fig. 9(a). A TSTM system mainly comprises four parts: the free deformation test, the restraint test, the thermal control and the deformation control. The free deformation test is the ADTM test, which aims for measurement of the AD as described in Section 2.1.1 (Fig. 5). The restraint test is the main part of the TSTM system. In the restraint test, a dog-bone specimen, which has the similar geometry to that of the ADTM test, is restrained by actively applying a force F at one end of the specimen. The value of F is determined by a feedback loop (FL1) to fulfill the deformation control, which keeps adjusting the F to make the deformation ε_r in the straight part of the specimen constant. Both the free and restrained specimens are connected to a cryostat, which keeps adjusting the water temperature T_w to keep the temperature in the specimen T_c following a pre-specified constant value or profile, with a specially designed feedback loop FL2. An example of such a TSTM is shown in Fig. 9(b).

In line with Fig. 9(a), some representative TSTMs in the past four decades are summarized in Table .2, distinguishing the specific differences between TSTMs in specimen size, strain measurement methods, strain control algorithms, and time-zero settings. All selected TSTMs use specimens longer than 1000 mm. For strain measurement, TSTMs all have different methods, but it is worth noting that the TSTM from University of Adelaide and University of Tokyo both arranged LVDT on top side of the specimen, which was reported to have better measurement accuracy and promote pre-installation efficiency. For the strain control (i.e., FL 1 in Fig. 9(a)), only the TSTM at the TU Delft uses a proportional–integral–derivative (PID) controller, which continuously adjust the load F according to the deformation measurement ε_r to fulfill the restraint condition, while others use stepping control which requires the load adjustment whenever the change of measured deformation exceeds a certain threshold. Finally, it is also interesting that different TSTMs have different time-zeros, either defined by the minimum EAS or by specifying the setting time. It is worth noting that, definition of time-zero was also broadly discussed by studies of AD, as introduced in Section 2.1.1, which can be avoided if the EAS results are available.

Despite providing valuable data about EAS, the TSTM faces certain challenges when it comes to practical implementation. Some major concerns are discussed as follows:

1 Due to the complexity of TSTM systems, the pre-test installation, casting, and post-test disassembling procedures demand a substantial workforce (Nguyen et al., 2019). For instance, the TSTM test

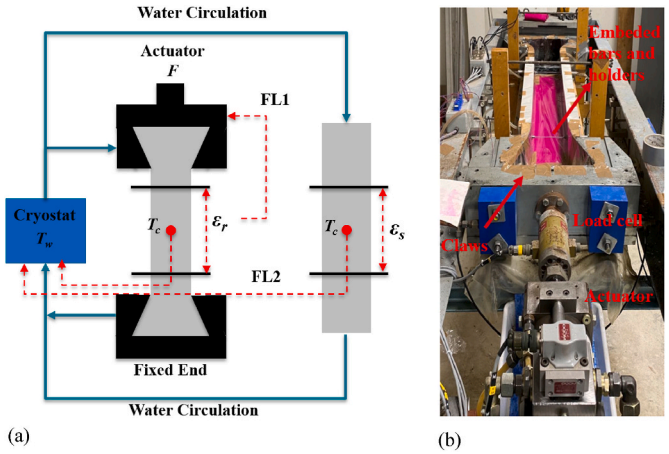

Fig. 9. TSTM systems: (a) a general schematic diagram; (b) the TSTM at the TU Delft, designed in Lokhorst (2001).

Table 2
Summary of representative TSTMs (Liang et al., 2023b).

Source	Year	L*W*H (mm)	Strain Measurement	Strain Control	Time-Zero
TUM (Springenschmid et al., 1994)	1984	1500 *150*150	Two-side, 2 LVDTs	Stepping	Stress 0.01 MPa
Israel IT (Igarashi et al., 2000), Hohai U (Shen et al., 2016)	1990, 2015	1500*150*150	Free-end, 1 LVDT	Stepping	Stress 0.01 MPa
NTNU (Klausen, 2016; Bjøntegaard, 1999)	1995, 2012	1000*88*100	Two-side, 4 LVDTs	Stepping	Initial setting
TU Delft (Lokhorst, 2001)	2000	1450*150*100	Two-side, 4 LVDTs	PID	Setting time
UQ (Nguyen et al., 2019)	2018	1200*80*80	Top-side, 4 LVDTs	Stepping	Setting time
UTokyo (Ou et al., 2023)	2022	1200*120*120	Top-side 2 LVDTs at two ends before 24 h and two-side 2 LVDTs afterward	Stepping	Setting time

conducted at TU Delft necessitates the collaboration of 3–4 individuals over a span of 2 entire working days, with each day consisting of 8 h (Lokhorst, 2001).

2 The choice of threshold value in TSTMs employing stepping control to achieve full restraint is frequently subjective and has the potential to impact the accuracy of the testing process (Xin et al., 2020; Staquet et al., 2012).

3 The positioning of LVDTs for strain measurement, which provides input for the feedback loop for the actuator (i.e., FL1 in Fig. 9(a)), plays a crucial role in ensuring the credibility of TSTM systems (Staquet et al., 2012). Consequently, recent studies on enhanced TSTMs have placed significant emphasis on this aspect (Nguyen et al., 2019; Ou et al., 2023). By analyzing the TSTMs outlined in Table 1, certain key points have emerged regarding the arrangement of LVDTs for strain measurement: 1) Rather than measuring deformation only on one side of the specimen, it is advisable to measure it on both sides. This approach enables the detection of potential eccentric deformations; 2) Instead of measuring deformation at the cross-head of the dog-bone specimen, it is preferable to measure it at the straight part. The absence of stress concentration in this region ensures more reliable results, which can be used as input for numerical models; 3) It is crucial to avoid directly attaching the LVDTs to the loading grip. Otherwise, any slip between the loading grip and the specimen will also be included in the strain measurement, resulting in possible errors.

4 In existing TSTMs, where specimens are tested horizontally, friction between the hardened specimen and the mold at the bottom can introduce errors in stress measurement. Proposed measures to reduce friction include using Teflon sheets (Nguyen et al., 2019) and implementing roller supports (Ou et al., 2023).

4.1.2. Influencing factors

Despite the aforementioned concerns, TSTMs still led to important findings. Igarashi et al. (2000) found that the AD-induced EAC happened when the stress-strength ratio reached 50%, and they pointed out the significant influence of relaxation on EAS evolution. Note that the strength data used in the calculation of stress-strength ratio refer to strength data obtained in traditional strength test (e.g., direct tensile strength test or tensile-splitting test), rather than the real strength of the specimen that is in the TSTM test. The importance of relaxation was also highlighted by other studies (Li et al., 2020b; Azenha et al., 2021). Zhu et al. (2020b) found that the EAC induced by thermal deformation happened when the stress-strength ratio reached 76%, and proposed a combined stress-strain failure criterion for evaluation of EAC risk. Despite that the failure mechanisms of restrained aging concrete are different with that under uniaxial tension test, a comprehensive review summarized that most EAC happens at a tensile stress-strength ratio of 0.5–0.9 (Zhu et al., 2021), and therefore the ratio of 0.5 is often adopted in structural designs to prevent EAC.

In some other more specific failure criterions of EAC, which are mostly a variant of the stress-strength ratio, the EAS remains a necessary input (Xin et al., 2021). Besides, with TSTM, the influence of temperature on AD-induced EAC was more systematically investigated. Lura et al. (2001) found that the temperature increase does not induce higher AD, but led to higher AD rate and higher EAS. Similar observations were obtained by Li et al. (2021a). Klausen et al. (2022) conducted comprehensive TSTM tests on various influencing factors, and concluded that temperature and the restraint degree remain to be the most influential factors. Moreover, they also emphasized the considerable variation between different batches of the same cement, which is similarly described in corrugated tube test for AD (Wyrzykowski et al., 2017). In addition, a number of TSTM-based tests were about the influence of mixture parameters, such as SCMs like GGBFS (Liang et al., 2023a; Shen et al., 2020b; Darquennes et al., 2011b,c; Markandeya et al., 2018), FA (Xin et al., 2022; Zhao et al., 2019b), and SF (Ji and Kanstad, 2018), alkali-activated materials (Li et al., 2020b), recycled aggregates (Bendimerad et al., 2020), and MgO expansive agent (Wang et al., 2022).

4.2. EAS model: modelling the EAS using AD and viscoelastic properties as input

Modelling the EAS basically requires three inputs: the AD, the creep/relaxation, and the elastic modulus. With the measurement or modelling results of AD and viscoelastic properties, as introduced in sections 2.0 and 3.0, the prediction of EAS should be straightforward by calculating the integral as in Eq. (5). The last key point is the conversion from the measured creep compliance to the relaxation modulus. Such conversion can be done by solving the integral relation between creep and relaxation (Eq. (3)) numerically (Bažant and Jirásek, 2018) as below:

$$R(t_0,1)=0 \tag{6-1}$$

$$R(t_0,2)=\frac{1}{J(t_0,t_0)} \tag{6-2}$$

$$R(t_0,k+1)=R(t_0,k)-\frac{1}{J_{k,k+1}}\sum_{i=1}^{k-1}\Delta J_{i,k}(R(t_0,i+1)-R(t_0,i)) \tag{6-3}$$

$$J_{k,k+1}=\frac{J(k+1,k+1)+J(k,k+1)}{2} \tag{6-4}$$

$$\Delta J_{i,k}=J(k,k+1)-J(k,k) \tag{6-5}$$

in which t is the loading time; t_0 is the time when load is applied; k is the time step equal to 1, 2, …, t. Note that the numerical procedures Eqs. (6-1)~(6-5) need to be implemented for every t_0 to obtain the full relaxation modulus R (t_0,t) as input for the EAS calculation. To avoid the complexity of such procedures, one can also use a semi-empirical solution given by Bazant and Kim (Bažant and Kim, 1979). Different from Eqs. 6-1)~(6-5, which was derived based on a linear superposition of creep/relaxation (Eq. (2)), Wittmann and van Breugel et al. (Li et al., 2020b; Wittmann, 1974; Van Breugel, 1980) obtained another conversion function, which is significantly easier than Eqs. (6-1)~(6-5). Such form started by assuming the total strain ε is composed of an elastic part

ε_{el} and a creep part ε_c. Under the boundary condition of a relaxation process, the total strain ε should be zero:

$$\varepsilon_{el} + \varepsilon_c = 0 \tag{7-1}$$

Express the elastic strain ε_{el} by Hooke's Law and take the derivative with respect to time, one gets:

$$\frac{1}{E(t_0)}\frac{d\sigma}{dt} = -\frac{d\varepsilon_c}{dt} \tag{7-2}$$

Assuming that the non-aging creep at a specific t_0 follows a power law function (i.e., $J(t\text{-}t_0) = a(t\text{-}t_0)^n$), Eqs. (7)–(2) can be rewritten as:

$$\frac{1}{E(t_0)}\frac{d\sigma}{dt} = -\sigma a n (t - t_0)^{n-1} \tag{7-3}$$

Integrating Eqs. (7)–(3) and assuming the initial stress is σ_0, one gets the ratio between the stress σ and initial stress σ_0:

$$\frac{\sigma}{\sigma_0} = e^{-E(t_0)a(t-t_0)^n} \tag{7-4}$$

which can be rewritten as the form of relaxation modulus:

$$R(t_0, t) = e^{1-J(t_0,t)E(t_0)}E(t_0) \tag{7-5}$$

Note that the exponent in Eqs. (7)–(5) is exactly the creep coefficient defined as the ratio of creep strain to elastic strain. Compared to Eqs. (6-1)~(6-5), Eqs. (7)–(5) is clearly a simpler way to obtain relaxation modulus. In recent years, both methods have shown good applicability in prediction of EAS. Wei et al. (2017b) converted the creep compliance given by the MPS theory using the conversion method of Eqs. (6-1)~(6-5), and successfully predicted the EAS under varying temperature in restrained concrete with good precision. On the other hand, using Eqs. (7)–(5), Li et al. (2020b, 2021b, 2022c) successfully predicted the EAS induced by restrained AD of alkali-activated material in multiple testing cases. In addition, it is also worth noting that some methods do not require to obtain the relaxation modulus and solve the integral in Eq. (5). Instead, it is also possible to simulate the EAS from the perspective of creep. For example, Klausen (2016) first calculated the incremental creep strain based on Eq. (2), and then assuming both the AD and thermal deformation were restrained, they calculated the incremental EAS with an elastic relation, which also matched well with the experimental observation.

Note that the models mentioned above about EAS were all based on a 1D restrained case, since the validation data is from the TSTM test, which is exactly an 1D restraint test. Modelling the EAS in real structures requires the use of FEM models. It should however be noted that directly implementing the linear viscoelastic constitutive relation as described by Eq. (2) or Eq. (5) in FEM is difficult, because the strain/stress history of every previous time step would need to be stored to do the linear superposition over the whole computation process, which is difficult for large models with a lot of meshes and degrees of freedom. Instead, the exponential algorithm (Bažant and Jirásek, 2018; Yu et al., 2012; Di Luzio et al., 2020) based on the rate-type form of Eq. (2) or Eq. (5) can circumvent such problem by changing the integral into a rate-type form and only requires to store some internal variables of the retardation chains across the calculation process. Based on the Kelvin chain model, the creep compliance function can be directly used as input to fit a continuous retardation chain (Bažant and Xi, 1995) and then the EAS evolution of any structures can be calculated by a proper boundary condition in FEM. Note that with the Kelvin chain model, the input is directly from the creep test and therefore the conversion from creep to relaxation is not needed either. Using the exponential algorithm with Kelvin chain, numerical studies have successfully predicted the EAS results of a TSTM test (Liu and Schindler, 2020; Liang et al., 2022a,b).

5. Conclusions

For many specially-designed cementitious materials, like HPC, UHPC, alkali activated materials, etc., which often have a very low internal RH and dense microstructure, AD-induced EAC risk is high. To evaluate and understand the EAC risk, the AD, viscoelastic properties, and EAS are the key points. This paper systematically reviewed relevant experimental and modelling methods and obtained the following findings:

1) The corrugated tube test allows for testing AD from the setting time and is sensitive enough to distinguish the influence of multiple factors on AD development, including the influence of temperature, cementitious materials, and various admixtures. Changing the corrugated tube size allows for AD tests of concrete. Multiple mitigation strategies including the use of more inert SCMs for controlling hydration, SRA for reducing surface tension in the pores, and internal curing either by light aggregate or SAPs, were proved to be effective in many studies.
2) The applicability of the maturity concept is questionable in prediction of AD under a varying temperature history. The influence of temperature on AD is complex because temperature not only leads to a change of hydration kinetics but also to changes in the internal RH, the surface tension, and the pore structure, which all significantly influences the self-desiccation process. It is clear that temperature increase leads to earlier onset of self-desiccation shrinkage and faster increase of EAS. However, it should also be noted that even at low-temperature, the magnitude of AD is still high, despite a later onset, and therefore the AD-induced EAC risk cannot be neglected.
3) The capillary pressure theory was proved by many studies to give a good prediction of self-desiccation shrinkage. The AD is the viscoelastic response of the microstructure to the capillary pressure, induced by RH drop in the hydration process. Therefore, incorporation of creep deformation in such models is important. In addition, another part of AD, which is induced by expansive products like ettringite, is often neglected in both modelling and experimental works, which can cause overestimation of EAS.
4) The viscoelastic properties, including the elastic modulus and creep, can both be tested with an in-situ hourly-repeated loading scheme. Such method leads to high-resolution measurement of the evolution of very early-age elastic modulus and creep, which are important inputs for EAS analysis.
5) The microscale mechanical tests, including the nanoindentation and microindentation tests, offered fundamental understandings of the elastic modulus and creep, and paved a way for multi-scale modelling. Either by micromechanical homogenization schemes (e.g., Mori-Tanaka or Self-Consistent) or microscale FEM models (e.g., Lattice fracture model), combined with a hydration model (e.g., CEMHYD3D or CEMHYD3D), the time-dependent evolution of elastic modulus and creep can be calculated. The viscoelastic properties are not only an important input for EAS, but also for AD at microscale, which is considered as the viscoelastic response of the microstructure to the internal capillary pressure.
6) The EAS evolution is the combined result of AD and viscoelastic properties. TSTM test can provide EAS results under different temperatures and restraint degrees. Besides, the AD of a dummy specimen with a similar geometry and temperature history as a TSTM specimen, which is called the ADTM in a TSTM system, can also be tested in free condition. Thus, the TSTM system provides a unified testing scheme of AD and EAS, which helps to build up the models of EAS.
7) With the experimental or modelling results of AD, elastic modulus, and creep, the EAS can be calculated by the integral of linear superposition. Conversion of creep function to relaxation function is often an important step. To run FEM analysis on EAC, the exponential algorithm based on the rate-type form is a more efficient method to avoid directly solving the integrals which requires storing huge amounts of internal variables.

8) Combining the modelling schemes reviewed in this paper, including the hydration models for volume change of hydrates, homogenization schemes (or FEMs) for upscaling of viscoelastic properties, and the capillary pressure theory for self-desiccation shrinkage, a unified model can be constructed, which enables to predict the EAS directly based on the composition of utilized mixtures.

6. Outlook

EAS is an important indicator of the EAC risk, and it is strongly dependent on the AD and viscoelastic properties. Therefore, experimental and numerical tools for EAC analysis should lay equal emphasis on AD, viscoelastic properties, and EAS to obtain a comprehensive understanding of EAC issues. Based on this review, following works should be considered for further improvement in the experimental and numerical tools for EAC analysis:

1) TSTM test should not only focus on the EAS and AD evolution, but also the evolution of viscoelastic properties, which are important input for EAS analysis and modelling. Rather than the strain-controlled test in the EAS measurement, an hourly-repeated loading scheme can be incorporated into the TSTM test to measure the viscoelastic properties at every hour. Thereby, the TSTM itself can be a unified testing system for the three important early-age properties/behaviors (AD, EAS, and viscoelastic properties) relevant to EAC.
2) The effects of temperature on AD should be further examined. Contradictory findings have been found in literatures regarding the influence of temperature on AD. The complexity of this issue is that AD not only influence the hydration kinetics, but also expansive hydration products like ettringite that leads to autogenous swelling and RH, porosity, and surface tension that significantly influences the self-desiccation process.
3) The efficiency of TSTM tests should be further improved. To obtain the AD, EAS, and viscoelastic properties, at least two TSTM tests should be conducted for each mixture. Moreover, considering the scatter in measurement of early-age AD and EAS, several repeated tests may also be needed for each mixture. Due to the complexity of current TSTM system, the cost of such a test is high and therefore more sustainable and efficient testing methods should be developed in order to obtain more testing data in a broad range of mixtures.
4) The modelling schemes of EAS should be further examined and developed. The lack of data for early-age viscoelastic properties is one of the main challenges in validating such models. Despite that solid theoretical basis is present, a systematic validation of these modelling schemes for predicting EAS is still missing. Therefore, a thorough investigation based on comprehensive and reliable input of viscoelastic properties is needed to validate or improve the applicability of EAS models.
5) Efficient and reliable data-driven models should be developed for analyzing the EAC risks. Due to the complexity of EAC issues, a unified model in this field requires to couple multiple physical and chemical mechanisms, including (but not limited to) hydration reaction, heat transfer, and viscoelastic mechanical response. The computational cost of solving such a complex multi-fields model is high. Building a surrogate model by data-driven approaches to replace the complex multi-fields model can promote the computational efficiency.

CRediT authorship contribution statement

Minfei Liang: Conceptualization, Formal analysis, Investigation, Methodology, Resources, Software, Visualization, Writing – original draft, Writing – review & editing. **Jinbao Xie:** Investigation, Visualization, Writing – review & editing. **Shan He:** Investigation, Methodology, Writing – review & editing. **Yu Chen:** Investigation, Writing – review & editing. **Erik Schlangen:** Conceptualization, Funding acquisition, Investigation, Supervision, Writing – review & editing, Project administration. **Branko Šavija:** Supervision, Writing – review & editing, Funding acquisition, Investigation, Project administration.

Declaration of competing interest

The authors declare that they have no known competing financial interests or personal relationships that could have appeared to influence the work reported in this paper.

Data availability

Data will be made available on request.

Acknowledgements

Minfei Liang and Jinbao Xie would like to acknowledge the funding supported by China Scholarship Council under the grant numbers 202007000027 and 202006260045, respectively. Branko Šavija acknowledges the financial support of the European Research Council (ERC) within the framework of the ERC Starting Grant Project "Auxetic Cementitious Composites by 3D printing (ACC-3D)", Grant Agreement Number 101041342.

References

AASHTO, 2012. AASHTO LRFD Bridge Design Specifications. American Association of State Highway and Transportation Officials, Washington DC.
Aili, A., Vandamme, M., Torrenti, J.-M., Masson, B., 2018. Is long-term autogenous shrinkage a creep phenomenon induced by capillary effects due to self-desiccation? Cement Concr. Res. 108, 186–200. https://doi.org/10.1016/j.cemconres.2018.02.023.
Aili, A., Vandamme, M., Torrenti, J.M., Masson, B., 2020. A viscoelastic poromechanical model for shrinkage and creep of concrete. Cement Concr. Res. 129, 105970 https://doi.org/10.1016/J.CEMCONRES.2019.105970.
Akcay, B., Tasdemir, M.A., 2009. Optimisation of using lightweight aggregates in mitigating autogenous deformation of concrete. Construct. Build. Mater. 23, 353–363. https://doi.org/10.1016/j.conbuildmat.2007.11.015.
American Concrete Institute, 2008. ACI Committee 209–Creep and Shrinkage., Guide for Modeling and Calculating Shrinkage and Creep in Hardened Concrete. American Concrete Institute.
American Concrete Institute Committee 209 (ACI), 1992. Prediction of Creep, Shrinkage, and Temperature Effects in Concrete Structures. ACI, Farmington Hills, MI, USA.
Amin, M.N., Kim, J.-S., Dat, T.T., Kim, J.-K., 2010. Improving test methods to measure early age autogenous shrinkage in concrete based on air cooling. IES J. Part A Civil Struct. Eng. 3, 244–256. https://doi.org/10.1080/19373260.2010.522314.
Atrushi, D.S., 2003. Tensile and Compressive Creep of Early Age Concrete. Testing and Modelling.
Ausweger, M., Binder, E., Lahayne, O., Reihsner, R., Maier, G., Peyerl, M., Pichler, B., 2019. Early-age evolution of strength, stiffness, and non-aging creep of concretes: experimental characterization and correlation analysis. Materials 12. https://doi.org/10.3390/ma12020207.
Awasthy, N., Schlangen, E., Hordijk, D., Šavija, B., Luković, M., 2023. The role of eigenstresses on apparent strength and stiffness of normal, high strength, and ultra-high performance fibre reinforced concrete. Dev. Built Environ. 16, 100277 https://doi.org/10.1016/j.dibe.2023.100277.
Azenha, M., Kanavaris, F., Schlicke, D., Jędrzejewska, A., Benboudjema, F., Honorio, T., Šmilauer, V., Serra, C., Forth, J., Riding, K., Khadka, B., Sousa, C., Briffaut, M., Lacarrière, L., Koenders, E., Kanstad, T., Klausen, A., Torrenti, J.M., Fairbairn, E.M. R., 2021. Recommendations of RILEM TC 287-CCS: thermo-chemo-mechanical modelling of massive concrete structures towards cracking risk assessment. Mater. Struct./Mater. Constr. 54, 135. https://doi.org/10.1617/s11527-021-01732-8.
Bal, L., Buyle-Bodin, F., 2013. Artificial neural network for predicting drying shrinkage of concrete. Construct. Build. Mater. 38, 248–254. https://doi.org/10.1016/J.CONBUILDMAT.2012.08.043.
Bal, L., Buyle-Bodin, F., 2014. Artificial neural network for predicting creep of concrete. Neural Comput. Appl. 25, 1359–1367. https://doi.org/10.1007/s00521-014-1623-z.
Barcelo, L., Moranville, M., Clavaud, B., 2005. Autogenous shrinkage of concrete: a balance between autogenous swelling and self-desiccation. Cement Concr. Res. 35, 177–183. https://doi.org/10.1016/j.cemconres.2004.05.050.
Baronet, J., Sorelli, L., Charron, J.P., Vandamme, M., Sanahuja, J., 2022. A two-scale method to rapidly characterize the logarithmic basic creep of concrete by coupling microindentation and uniaxial compression creep test. Cem. Concr. Compos. 125 https://doi.org/10.1016/j.cemconcomp.2021.104274.
Bažant, Z.P., Jirásek, M., 2018. Creep and Hygrothermal Effects in Concrete Structures. Springer Netherlands, Dordrecht. https://doi.org/10.1007/978-94-024-1138-6.

Bažant, Z.P., Kim, S.-S., 1979. Nonlinear creep of concrete—adaptation and flow. J. Eng. Mech. Div. 105, 429–446. https://doi.org/10.1061/JMCEA3.0002483.
Bažant, Z.R., Li, G.H., 2008. Comprehensive database on concrete creep and shrinkage. ACI Mater. J. 105 https://doi.org/10.14359/20206.
Bazant, Z.P., Osman, E., 1976. Double power law for basic creep of concrete. Matér. Constr. 9, 3–11.
Bazant, Z.P., Wu, S.T., 1974. Rate-type Creep Law of Aging Concrete Based on Maxwell Chain ER(t, r).
Bažant, Z.P., Xi, Y., 1995. Continuous retardation spectrum for solidification theory of concrete creep. J. Eng. Mech. 121, 281–288. https://doi.org/10.1061/(ASCE)0733-9399(1995)121:2(281).
Bazant, Z.P., Xi, Y., Baweja, S., 1995. Continuous retardation spectrum for solidification theory of aging creep of concrete. Proc. Eng. Mech. 2.
Bažant, Z.P., Cusatis, G., Cedolin, L., 2004. Temperature effect on concrete creep modeled by microprestress-solidification theory. J. Eng. Mech. 130, 691–699. https://doi.org/10.1061/(ASCE)0733-9399(2004)130:6(691).
Bendimerad, A.Z., Delsaute, B., Rozière, E., Staquet, S., Loukili, A., 2020. Advanced techniques for the study of shrinkage-induced cracking of concrete with recycled aggregates at early age. Construct. Build. Mater. 233, 117340 https://doi.org/10.1016/j.conbuildmat.2019.117340.
Bentur, A., Kovler, K., 2003. Evaluation of early age cracking characteristics in cementitious systems. Mater. Struct. 36, 183–190. https://doi.org/10.1007/BF02479556.
Bentur, A., Igarashi, S., Kovler, K., 2001. Prevention of autogenous shrinkage in high-strength concrete by internal curing using wet lightweight aggregates. Cement Concr. Res. 31, 1587–1591. https://doi.org/10.1016/S0008-8846(01)00608-1.
Bentz, D.P., Garboczi, E.J., Haecker, C.J., Jensen, O.M., 1999. Effects of cement particle size distribution on performance properties of Portland cement-based materials. Cement Concr. Res. 29, 1663–1671. https://doi.org/10.1016/S0008-8846(99)00163-5.
Bentz, D.P., Jensen, O.M., Hansen, K.K., Olesen, J.F., Stang, H., Haecker, C.-J., 2001. Influence of cement particle-size distribution on early age autogenous strains and stresses in cement-based materials. J. Am. Ceram. Soc. 84, 129–135. https://doi.org/10.1111/j.1151-2916.2001.tb00619.x.
Bernard, O., Ulm, F.-J., Lemarchand, E., 2003. A multiscale micromechanics-hydration model for the early-age elastic properties of cement-based materials. Cement Concr. Res. 33, 1293–1309. https://doi.org/10.1016/S0008-8846(03)00039-5.
Beushausen, H., Dittmer, T., 2015. The influence of aggregate type on the strength and elastic modulus of high strength concrete. Construct. Build. Mater. 74, 132–139. https://doi.org/10.1016/J.CONBUILDMAT.2014.08.055.
Bjøntegaard, Ø., 1999. Termal Dilation and Autogenous Deformation as Driving Forces to Self-Induced Stresses in High Performance Concrete. Ph.D. thesis. Norwegian University of Science and Technology (NTNU).
Bjøntegaard, Ø., Sellevold, E.J., 2001. Interaction between thermal dilation and autogenous deformation in high performance concrete. Mater. Struct. 34, 266–272. https://doi.org/10.1007/BF02482205.
Bouasker, M., Khalifa, N.E.H., Mounanga, P., Ben Kahla, N., 2014. Early-age deformation and autogenous cracking risk of slag–limestone filler-cement blended binders. Construct. Build. Mater. 55, 158–167. https://doi.org/10.1016/j.conbuildmat.2014.01.037.
Boulay, C., Staquet, S., Delsaute, B., Carette, J., Crespini, M., Yazoghli-Marzouk, O., Merliot, É., Ramanich, S., 2014. How to monitor the modulus of elasticity of concrete, automatically since the earliest age? Mater. Struct./Mater. Constr. 47, 141–155. https://doi.org/10.1617/s11527-013-0051-3.
Van Breugel, K., 1980. Relaxation of Young Concrete.
van Breugel, K., 1995. Numerical simulation of hydration and microstructural development in hardening cement-based materials (I) theory. Cement Concr. Res. 25, 319–331. https://doi.org/10.1016/0008-8846(95)00017-8.
Briffaut, M., Benboudjema, F., Torrenti, J.M., Nahas, G., 2012. Concrete early age basic creep: experiments and test of rheological modelling approaches. Construct. Build. Mater. 36, 373–380. https://doi.org/10.1016/j.conbuildmat.2012.04.101.
Briffaut, M., Benboudjema, F., D'Aloia, L., 2016. Effect of fibres on early age cracking of concrete tunnel lining. Part I: laboratory ring test. Tunn. Undergr. Space Technol. 59, 215–220. https://doi.org/10.1016/J.TUST.2016.07.016.
Brussels, B., 1986. Concrete Tests—Test Specimens—Part 2: Making and Curing of Test Specimens for Strength Tests. International Organization for Standardization, Geneva, Switzerland. ISO/TC 71/SC 1 Test Methods for Concrete.
Van Bunderen, C., Snellings, R., Vandewalle, L., Cizer, Ö., 2019. Early-age hydration and autogenous deformation of cement paste containing flash calcined dredging sediments. Construct. Build. Mater. 200, 104–115. https://doi.org/10.1016/j.conbuildmat.2018.12.090.
Carette, J., Staquet, S., 2016. Monitoring and modelling the early age and hardening behaviour of eco-concrete through continuous non-destructive measurements: Part II. Mechanical behaviour. Cem. Concr. Compos. 73, 1–9. https://doi.org/10.1016/j.cemconcomp.2016.07.003.
Carette, J., Staquet, S., 2018. Unified modelling of the temperature effect on the autogenous deformations of cement-based materials. Cem. Concr. Compos. 94, 62–71. https://doi.org/10.1016/j.cemconcomp.2018.08.008.
Carette, J., Joseph, S., Cizer, Ö., Staquet, S., 2018. Decoupling the autogenous swelling from the self-desiccation deformation in early age concrete with mineral additions: micro-macro observations and unified modelling. Cem. Concr. Compos. 85, 122–132. https://doi.org/10.1016/j.cemconcomp.2017.10.008.
Carol, I., Bažant, Z.P., 1993. Viscoelasticity with aging caused by solidification of nonaging constituent. J. Eng. Mech. 119, 2252–2269. https://doi.org/10.1061/(ASCE)0733-9399(1993)119:11(2252).
Charpin, L., Le Pape, Y., Coustabeau, É., Toppani, É., Heinfling, G., Le Bellego, C., Masson, B., Montalvo, J., Courtois, A., Sanahuja, J., Reviron, N., 2018. A 12 year EDF study of concrete creep under uniaxial and biaxial loading. Cement Concr. Res. 103, 140–159. https://doi.org/10.1016/j.cemconres.2017.10.009.
Chen, Y., Wei, J., Huang, H., Jin, W., Yu, Q., 2018. Application of 3D-DIC to characterize the effect of aggregate size and volume on non-uniform shrinkage strain distribution in concrete. Cem. Concr. Compos. 86, 178–189. https://doi.org/10.1016/j.cemconcomp.2017.11.005.
Chen, X., Hou, D., Han, Y., Ding, X., Hua, P., 2021. Clustering analysis of grid nanoindentation data for cementitious materials. J. Mater. Sci. 56, 12238–12255. https://doi.org/10.1007/s10853-021-05848-8.
Chen, Y., Liang, M., Zhang, Y., Li, Z., Šavija, B., Schlangen, E., Çopuroğlu, O., 2023. Can superabsorbent polymers be used as rheology modifiers for cementitious materials in the context of 3D concrete printing? Construct. Build. Mater. 371, 130777 https://doi.org/10.1016/j.conbuildmat.2023.130777.
Chu, I., Kwon, S.H., Amin, M.N., Kim, J.-K., 2012. Estimation of temperature effects on autogenous shrinkage of concrete by a new prediction model. Construct. Build. Mater. 35, 171–182. https://doi.org/10.1016/j.conbuildmat.2012.03.005.
Constantinides, G., Ulm, F.J., 2004. The effect of two types of C-S-H on the elasticity of cement-based materials: results from nanoindentation and micromechanical modeling. Cement Concr. Res. 34, 67–80. https://doi.org/10.1016/S0008-8846(03)00230-8.
Dabarera, A., Li, L., Dao, V., 2021. Experimental evaluation and modelling of early-age basic tensile creep in high-performance concrete. Mater. Struct./Mater. Constr. 54 https://doi.org/10.1617/s11527-021-01722-w.
Darquennes, A., Staquet, S., Espion, B., 2011a. Determination of time-zero and its effect on autogenous deformation evolution. Eur. J. Environ. Civil Eng. 15, 1017–1029. https://doi.org/10.1080/19648189.2011.9695290.
Darquennes, A., Staquet, S., Delplancke-Ogletree, M.P., Espion, B., 2011b. Effect of autogenous deformation on the cracking risk of slag cement concretes. Cem. Concr. Compos. 33, 368–379. https://doi.org/10.1016/j.cemconcomp.2010.12.003.
Darquennes, A., Staquet, S., Espion, B., 2011c. Behaviour of slag cement concrete under restraint conditions. Eur. J. Environ. Civil Eng. 15, 787–798. https://doi.org/10.1080/19648189.2011.9693365.
Delsaute, B., Boulay, C., Staquet, S., 2016. Creep testing of concrete since setting time by means of permanent and repeated minute-long loadings. Cem. Concr. Compos. 73, 75–88. https://doi.org/10.1016/J.CEMCONCOMP.2016.07.005.
Delsaute, B., Torrenti, J.M., Staquet, S., 2017. Modeling basic creep of concrete since setting time. Cem. Concr. Compos. 83, 239–250. https://doi.org/10.1016/j.cemconcomp.2017.07.023.
Delsaute, B., Torrenti, J.M., Staquet, S., 2021. Prediction of the basic creep of concrete with high substitution of Portland cement by mineral additions at early age. Struct. Concr. 22, E563–E580. https://doi.org/10.1002/suco.201900313.
EN, 2002. EN 1992-1-1 Eurocode 2: Design of Concrete Structures—Part 1-1: General Ruels and Rules for Buildings. CEN, Brussels, Belgium.
F. Hansen, P., Pedersen, J., 1977. Maturity computer for controlled curing and hardening of concrete. Nordisk Betong 1, 19–34.
Fairbairn, E.M.R., Azenha, M. (Eds.), 2019. Thermal Cracking of Massive Concrete Structures. Springer International Publishing, Cham. https://doi.org/10.1007/978-3-319-76617-1.
Fang, G., Wang, Q., Zhang, M., 2021. Micromechanical analysis of interfacial transition zone in alkali-activated fly ash-slag concrete. Cem. Concr. Compos. 119, 103990 https://doi.org/10.1016/j.cemconcomp.2021.103990.
Farah, M., Grondin, F., Alam, S.Y., Loukili, A., 2019. Experimental approach to investigate creep-damage bilateral effects in concrete at early age. Cem. Concr. Compos. 96, 128–137. https://doi.org/10.1016/j.cemconcomp.2018.11.022.
Feng, S., Lyu, J., Xiao, H., Feng, J., 2022. Application of cellulose fibre in ultra-high-performance concrete to mitigate autogenous shrinkage. J Sustain Cem Based Mater 1–14. https://doi.org/10.1080/21650373.2022.2119618.
fib, 2013. fib Model Code for Concrete Structures 2010. Wiley-VCH Verlag GmbH & Co. KGaA, Weinheim, Germany. https://doi.org/10.1002/9783433604090.
Filho, J.R.T., de Araújo, M.A.P.G., Snoeck, D., De Belie, N., 2019. Discussing different approaches for the time-zero as start for autogenous shrinkage in cement pastes containing superabsorbent polymers. Materials 12. https://doi.org/10.3390/ma12182962.
Frech-Baronet, J., Sorelli, L., Charron, J.P., 2017. New evidences on the effect of the internal relative humidity on the creep and relaxation behaviour of a cement paste by micro-indentation techniques. Cement Concr. Res. 91, 39–51. https://doi.org/10.1016/J.CEMCONRES.2016.10.005.
Gan, Y., Vandamme, M., Zhang, H., Chen, Y., Schlangen, E., van Breugel, K., Šavija, B., 2020. Micro-cantilever testing on the short-term creep behaviour of cement paste at micro-scale. Cement Concr. Res. 134 https://doi.org/10.1016/j.cemconres.2020.106105.
Gan, Y., Romero Rodriguez, C., Zhang, H., Schlangen, E., van Breugel, K., Šavija, B., 2021. Modeling of microstructural effects on the creep of hardened cement paste using an experimentally informed lattice model. Comput. Aided CivilInfrastruct. Eng. 36, 560–576. https://doi.org/10.1111/mice.12659.
Gandomi, A.H., Sajedi, S., Kiani, B., Huang, Q., 2016. Genetic programming for experimental big data mining: a case study on concrete creep formulation. Autom. ConStruct. 70, 89–97. https://doi.org/10.1016/j.autcon.2016.06.010.
Gao, Y., Zhang, J., Han, P., 2013. Determination of stress relaxation parameters of concrete in tension at early-age by ring test. Construct. Build. Mater. 41, 152–164. https://doi.org/10.1016/J.CONBUILDMAT.2012.12.004.
Gao, P., Chen, Y., Huang, H., Qian, Z., Schlangen, E., Wei, J., Yu, Q., 2021. Effect of coarse aggregate size on non-uniform stress/strain and drying-induced

microcracking in concrete. Compos. B Eng. 216 https://doi.org/10.1016/j.compositesb.2021.108880.
Gao, P., Ye, G., Huang, H., Qian, Z., Schlangen, E., Wei, J., Yu, Q., 2022. Incorporating elastic and creep deformations in modelling the three-dimensional autogenous shrinkage of cement paste. Cement Concr. Res. 160, 106907 https://doi.org/10.1016/J.CEMCONRES.2022.106907.
Geng, D., Dai, N., Jin, X., Miao, E., 2021. Comparison of calculating methods and applications of different concrete maturity. J. Phys. Conf. Ser. 2011, 012022 https://doi.org/10.1088/1742-6596/2011/1/012022.
Ghafari, E., Ghahari, S.A., Costa, H., Júlio, E., Portugal, A., Durães, L., 2016. Effect of supplementary cementitious materials on autogenous shrinkage of ultra-high performance concrete. Construct. Build. Mater. 127, 43–48. https://doi.org/10.1016/J.CONBUILDMAT.2016.09.123.
Göbel, L., Bos, C., Schwaiger, R., Flohr, A., Osburg, A., 2018. Micromechanics-based investigation of the elastic properties of polymer-modified cementitious materials using nanoindentation and semi-analytical modeling. Cem. Concr. Compos. 88, 100–114. https://doi.org/10.1016/j.cemconcomp.2018.01.010.
Gu, C., Wang, Y., Gao, F., Yang, Y., Ni, T., Liu, J., Lou, X., Chen, J., 2019. Early age tensile creep of high performance concrete containing mineral admixtures: experiments and modeling. Construct. Build. Mater. 197, 766–777. https://doi.org/10.1016/j.conbuildmat.2018.11.218.
He, Z., Zhan, P., Du, S., Liu, B., Yuan, W., 2019. Creep behavior of concrete containing glass powder. Compos. B Eng. 166, 13–20. https://doi.org/10.1016/j.compositesb.2018.11.133.
Hedegaard, B., 2020. Creep and shrinkage modeling of concrete using solidification theory. J. Mater. Civil Eng. 32, 04020179 https://doi.org/10.1061/(asce)mt.1943-5533.0003256.
Hedegaard, B.D., Shield, C.K., French, C.E.W., 2015. Smeared-bar model for viscoelastic analysis of uncracked reinforced concrete structures. J. Struct. Eng. 141, 04014167 https://doi.org/10.1061/(asce)st.1943-541x.0001124.
Hilaire, A., Benboudjema, F., Darquennes, A., Berthaud, Y., Nahas, G., 2013. Analysis of concrete creep in compression, tension and bending: numerical modeling. In: Mechanics and Physics of Creep, Shrinkage, and Durability of Conrete: A Tribute to Zdenek P. Bazant - Proceedings of the 9th Int. Conf. On Creep, Shrinkage, and Durability Mechanics, CONCREEP 2013. American Society of Civil Engineers (ASCE), pp. 348–355. https://doi.org/10.1061/9780784413111.041.
Hill, R., 1965. A self-consistent mechanics of composite materials. J. Mech. Phys. Solid. 13, 213–222. https://doi.org/10.1016/0022-5096(65)90010-4.
Hilloulin, B., Tran, V.Q., 2022. Using machine learning techniques for predicting autogenous shrinkage of concrete incorporating superabsorbent polymers and supplementary cementitious materials. J. Build. Eng. 49, 104086 https://doi.org/10.1016/j.jobe.2022.104086.
Honorio, T., Bary, B., Benboudjema, F., 2016. Multiscale estimation of ageing viscoelastic properties of cement-based materials: a combined analytical and numerical approach to estimate the behaviour at early age. Cement Concr. Res. 85, 137–155. https://doi.org/10.1016/j.cemconres.2016.03.010.
Hu, Z., Shi, C., Cao, Z., Ou, Z., Wang, D., Wu, Z., He, L., 2013. A review on testing methods for autogenous shrinkage measurement of cement-based materials. J. Sustain. Cem. Based Mater. 2, 161–171. https://doi.org/10.1080/21650373.2013.797937.
Hu, Z., Wyrzykowski, M., Scrivener, K., Lura, P., 2019a. Prediction of autogenous shrinkage of cement pastes as poro-visco-elastic deformation. Cement Concr. Res. 126 https://doi.org/10.1016/j.cemconres.2019.105917.
Hu, Z., Hilaire, A., Ston, J., Wyrzykowski, M., Lura, P., Scrivener, K., 2019b. Intrinsic viscoelasticity of C-S-H assessed from basic creep of cement pastes. Cement Concr. Res. 121, 11–20. https://doi.org/10.1016/j.cemconres.2019.04.003.
Hu, Z., Wyrzykowski, M., Griffa, M., Scrivener, K., Lura, P., 2020a. Young's modulus and creep of calcium-silicate-hydrate compacts measured by microindentation. Cement Concr. Res. 134 https://doi.org/10.1016/j.cemconres.2020.106104.
Hu, Z., Hilaire, A., Wyrzykowski, M., Lura, P., Scrivener, K., 2020b. Visco-elastic behavior of blended cement pastes at early ages. Cem. Concr. Compos. 107, 103497 https://doi.org/10.1016/J.CEMCONCOMP.2019.103497.
Huang, H., Ye, G., 2017. Examining the "time-zero" of autogenous shrinkage in high/ultra-high performance cement pastes. Cement Concr. Res. 97, 107–114. https://doi.org/10.1016/J.CEMCONRES.2017.03.010.
Huang, H., Garcia, R., Huang, S.S., Guadagnini, M., Pilakoutas, K., 2019. A practical creep model for concrete elements under eccentric compression. Mater. Struct./Mater. Construct. 52 https://doi.org/10.1617/s11527-019-1432-z.
Huang, L., Chen, Z., Ye, H., 2020. A mechanistic model for the time-dependent autogenous shrinkage of high performance concrete. Construct. Build. Mater. 255 https://doi.org/10.1016/j.conbuildmat.2020.119335.
Huang, D., Chen, P., Peng, H., Yang, Y., Yuan, Q., Su, M., 2021. A review and comparison study on drying shrinkage prediction between alkali-activated fly ash/slag and ordinary Portland cement. Construct. Build. Mater. 305, 124760 https://doi.org/10.1016/j.conbuildmat.2021.124760.
Hubler, M.H., Wendner, R., Bažant, Z.P., 2015a. Statistical justification of Model B4 for drying and autogenous shrinkage of concrete and comparisons to other models. Mater. Struct. 48, 797–814. https://doi.org/10.1617/s11527-014-0516-z.
Hubler, M.H., Wendner, R., Bažant, Z.P., 2015b. Comprehensive database for concrete creep and shrinkage: analysis and recommendations for testing and recording. ACI Mater. J. 112, 547–558. https://doi.org/10.14359/51687452.
Igarashi, S., Bentur, A., Kovler, K., 2000. Autogenous shrinkage and induced restraining stresses in high-strength concretes. Cement Concr. Res. 30, 1701–1707. https://doi.org/10.1016/S0008-8846(00)00399-9.
Irfan-ul-Hassan, M., Pichler, B., Reihsner, R., Hellmich, Ch, 2016. Elastic and creep properties of young cement paste, as determined from hourly repeated minute-long quasi-static tests. Cement Concr. Res. 82, 36–49. https://doi.org/10.1016/j.cemconres.2015.11.007.
Jensen, O.M., Hansen, P.F., 1999. Influence of temperature on autogenous deformation and relative humidity change in hardening cement paste. Cement Concr. Res. 29, 567–575. https://doi.org/10.1016/S0008-8846(99)00021-6.
Ji, G.M., Kanstad, T., 2018. Bjøntegaard, calibration of material models against TSTM test for crack risk assessment of early-age concrete containing fly ash. Adv. Mater. Sci. Eng. 2018 https://doi.org/10.1155/2018/1069181.
Jiang, C., Yang, Y., Wang, Y., Zhou, Y., Ma, C., 2014a. Autogenous shrinkage of high performance concrete containing mineral admixtures under different curing temperatures. Construct. Build. Mater. 61, 260–269. https://doi.org/10.1016/J.CONBUILDMAT.2014.03.023.
Jiang, W., De Schutter, G., Yuan, Y., 2014b. Degree of hydration based prediction of early age basic creep and creep recovery of blended concrete. Cem. Concr. Compos. 48, 83–90. https://doi.org/10.1016/j.cemconcomp.2013.10.012.
Jirásek, M., Havlásek, P., 2014. Accurate approximations of concrete creep compliance functions based on continuous retardation spectra. Comput. Struct. 135, 155–168. https://doi.org/10.1016/J.COMPSTRUC.2014.01.024.
Justs, J., Wyrzykowski, M., Bajare, D., Lura, P., 2015. Internal curing by superabsorbent polymers in ultra-high performance concrete. Cement Concr. Res. 76, 82–90. https://doi.org/10.1016/J.CEMCONRES.2015.05.005.
Klausen, A.E., 2016. Early Age Crack Assessment of Concrete Structures, Experimental Determination of Decisive Parameters. Ph.D. thesis. NTNU.
Klausen, A.E., Kanstad, T., 2021. The effect of shrinkage reducing admixtures on drying shrinkage, autogenous deformation, and early age stress development of concrete. Struct. Concr. 22 https://doi.org/10.1002/suco.201900583.
Klausen, A.E., Kanstad, T., Bjøntegaard, Ø., Sellevold, E., 2017. Comparison of tensile and compressive creep of fly ash concretes in the hardening phase. Cement Concr. Res. 95, 188–194. https://doi.org/10.1016/j.cemconres.2017.02.018.
Klausen, A.E., Kanstad, T., Bjøntegaard, Ø., 2019. Hardening concrete exposed to realistic curing temperature regimes and restraint conditions: advanced testing and design methodology. Adv. Mater. Sci. Eng. 2019. https://doi.org/10.1155/2019/9071034.
Klausen, A.E., Kanstad, T., Bjøntegaard, Ø., Sellevold, E.J., 2020. The effect of curing temperature on autogenous deformation of fly ash concretes. Cem. Concr. Compos. 109, 103574 https://doi.org/10.1016/j.cemconcomp.2020.103574.
Klausen, A.E., Kanstad, T., Bjøntegaard, Ø., 2022. The cracking risk of hardening concrete exposed to realistic curing temperature regimes and restraint conditions – experimental investigations of important parameters. Construct. Build. Mater. 338, 127662 https://doi.org/10.1016/J.CONBUILDMAT.2022.127662.
Klemczak, B., Żmij, A., 2019. Reliability of standard methods for evaluating the early-age cracking risk of thermal-shrinkage origin in concrete walls. Construct. Build. Mater. 226, 651–661. https://doi.org/10.1016/j.conbuildmat.2019.07.167.
Klug, P., Wittmann, F., 1974. Activation energy and activation volume of creep of hardened cement paste. Mater. Sci. Eng. 15, 63–66. https://doi.org/10.1016/0025-5416(74)90030-5.
Koenders, E.A.B., van Breugel, K., 1997. Numerical modelling of autogenous shrinkage of hardening cement paste. Cement Concr. Res. 27, 1489–1499. https://doi.org/10.1016/S0008-8846(97)00170-1.
Königsberger, M., Honório, T., Sanahuja, J., Delsaute, B., Pichler, B.L.A., 2021. Homogenization of nonaging basic creep of cementitious materials: a multiscale modeling benchmark. Construct. Build. Mater. 290, 123144 https://doi.org/10.1016/j.conbuildmat.2021.123144.
Krishnya, S., Yoda, Y., Elakneswaran, Y., 2021. A two-stage model for the prediction of mechanical properties of cement paste. Cem. Concr. Compos. 115, 103853 https://doi.org/10.1016/J.CEMCONCOMP.2020.103853.
Lai, M.H., Binhowimal, S.A.M., Griffith, A.M., Hanzic, L., Wang, Q., Chen, Z., Ho, J.C.M., 2021. Shrinkage design model of concrete incorporating wet packing density. Construct. Build. Mater. 280, 122448 https://doi.org/10.1016/j.conbuildmat.2021.122448.
Lavergne, F., Barthélémy, J.F., 2020. Confronting a refined multiscale estimate for the aging basic creep of concrete with a comprehensive experimental database. Cement Concr. Res. 136 https://doi.org/10.1016/j.cemconres.2020.106163.
Lee, K.M., Park, J.H., 2008. A numerical model for elastic modulus of concrete considering interfacial transition zone. Cement Concr. Res. 38, 396–402. https://doi.org/10.1016/J.CEMCONRES.2007.09.019.
Lee, K.M., Lee, H.K., Lee, S.H., Kim, G.Y., 2006. Autogenous shrinkage of concrete containing granulated blast-furnace slag. Cement Concr. Res. 36, 1279–1285. https://doi.org/10.1016/J.CEMCONRES.2006.01.005.
Li, Z., Nedeljković, M., Chen, B., Ye, G., 2019a. Mitigating the autogenous shrinkage of alkali-activated slag by metakaolin. Cement Concr. Res. 122, 30–41. https://doi.org/10.1016/j.cemconres.2019.04.016.
Li, Y., Li, Y., Wang, R., 2019b. Quantitative evaluation of elastic modulus of concrete with nanoidentation and homogenization method. Construct. Build. Mater. 212, 295–303. https://doi.org/10.1016/j.conbuildmat.2019.04.002.
Li, Z., Lu, T., Liang, X., Dong, H., Ye, G., 2020a. Mechanisms of autogenous shrinkage of alkali-activated slag and fly ash pastes. Cement Concr. Res. 135 https://doi.org/10.1016/j.cemconres.2020.106107.
Li, Z., Zhang, S., Liang, X., Ye, G., 2020b. Cracking potential of alkali-activated slag and fly ash concrete subjected to restrained autogenous shrinkage. Cem. Concr. Compos. 114 https://doi.org/10.1016/j.cemconcomp.2020.103767.
Li, L., Dao, V., Lura, P., 2021a. Autogenous deformation and coefficient of thermal expansion of early-age concrete: initial outcomes of a study using a newly-developed Temperature Stress Testing Machine. Cem. Concr. Compos. 119, 103997 https://doi.org/10.1016/j.cemconcomp.2021.103997.

Li, Z., Lu, T., Chen, Y., Wu, B., Ye, G., 2021b. Prediction of the autogenous shrinkage and microcracking of alkali-activated slag and fly ash concrete. Cem. Concr. Compos. 117 https://doi.org/10.1016/j.cemconcomp.2020.103913.
Li, Y., Chen, J., Wen, L., Wang, J., Li, K., 2021c. Investigation of the nonlinear creep of concrete with different initial defect rates under continuous compression with acoustic emission technology. J. Mater. Civil Eng. 33, 04020441 https://doi.org/10.1061/(asce)mt.1943-5533.0003550.
Li, J., Zhang, W., Monteiro, P.J.M., 2021d. Preferred orientation of calcium aluminosilicate hydrate compacts: implications for creep and indentation. Cement Concr. Res. 143, 106371 https://doi.org/10.1016/J.CEMCONRES.2021.106371.
Li, K., Long, Y., Wang, H., Wang, Y.-F., 2021e. Modeling and sensitivity analysis of concrete creep with machine learning methods. J. Mater. Civil Eng. 33, 04021206 https://doi.org/10.1061/(asce)mt.1943-5533.0003843.
Li, Y., Liu, Y., Li, Y., Li, Y., Wang, R., 2021f. Evaluation of concrete creep properties based on indentation test and multiscale homogenization method. Cem. Concr. Compos. 123, 104135 https://doi.org/10.1016/J.CEMCONCOMP.2021.104135.
Li, L., Dabarera, A.G.P., Dao, V., 2022a. Basic tensile creep of concrete with and without superabsorbent polymers at early ages. Construct. Build. Mater. 320, 126180 https://doi.org/10.1016/J.CONBUILDMAT.2021.126180.
Li, Y., Liu, Y., Wang, Z., Li, H., Mu, J., 2022b. Effect of phases on the creep properties of cement paste based on indentation test and homogenization scheme. Construct. Build. Mater. 317, 125957 https://doi.org/10.1016/j.conbuildmat.2021.125957.
Li, Z., Liang, X., Liu, C., Liang, M., van Breugel, K., Ye, G., 2022c. Thermal deformation and stress of alkali-activated slag concrete under semi-adiabatic condition: experiments and simulations. Cement Concr. Res. 159, 106887 https://doi.org/10.1016/j.cemconres.2022.106887.
Liang, S., Wei, Y., 2019. Methodology of obtaining intrinsic creep property of concrete by flexural deflection test. Cem. Concr. Compos. 97, 288–299. https://doi.org/10.1016/j.cemconcomp.2019.01.003.
Liang, S., Wei, Y., 2020a. New insights into creep and creep recovery of hardened cement paste at micro scale. Construct. Build. Mater. 248 https://doi.org/10.1016/j.conbuildmat.2020.118724.
Liang, S., Wei, Y., 2020b. Effects of water-to-cement ratio and curing age on microscopic creep and creep recovery of hardened cement pastes by microindentation. Cem. Concr. Compos. 113, 103619 https://doi.org/10.1016/j.cemconcomp.2020.103619.
Liang, S., Wei, Y., Wu, Z., 2017. Multiscale modeling elastic properties of cement-based materials considering imperfect interface effect. Construct. Build. Mater. 154, 567–579. https://doi.org/10.1016/j.conbuildmat.2017.07.196.
Liang, M., Li, Z., He, S., Chang, Z., Gan, Y., Schlangen, E., Šavija, B., 2022a. Stress evolution in restrained GGBFS concrete due to autogenous deformation: bayesian optimization of aging creep. Construct. Build. Mater. 324, 126690 https://doi.org/10.1016/J.CONBUILDMAT.2022.126690.
Liang, M., Chang, Z., He, S., Chen, Y., Gan, Y., Schlangen, E., Šavija, B., 2022b. Predicting early-age stress evolution in restrained concrete by thermo-chemo-mechanical model and active ensemble learning. Comput. Aided Civil Infrastruct. Eng. 37, 1809–1833. https://doi.org/10.1111/mice.12915.
Liang, M., Chang, Z., Wan, Z., Gan, Y., Schlangen, E., Šavija, B., 2022c. Interpretable Ensemble-Machine-Learning models for predicting creep behavior of concrete. Cem. Concr. Compos. 125, 104295 https://doi.org/10.1016/J.CEMCONCOMP.2021.104295.
Liang, M., Gan, Y., Chang, Z., Wan, Z., Schlangen, E., Šavija, B., 2022d. Microstructure-informed deep convolutional neural network for predicting short-term creep modulus of cement paste. Cement Concr. Res. 152, 106681 https://doi.org/10.1016/J.CEMCONRES.2021.106681.
Liang, M., Chang, Z., Zhang, Y., Cheng, H., He, S., Schlangen, E., Šavija, B., 2023a. Autogenous deformation induced- stress evolution in high-volume GGBFS concrete: macro-scale behavior and micro-scale origin. Construct. Build. Mater. 370, 130663 https://doi.org/10.1016/j.conbuildmat.2023.130663.
Liang, M., Chang, Z., Holthuizen, P., Chen, Y., He, S., Schlangen, E., Šavija, B., 2023b. Efficiently Assessing the Early-Age Cracking Risk of Cementitious Materials with A Mini Temperature Stress Testing Machine.
Liu, Z., Hansen, W., 2016. Aggregate and slag cement effects on autogenous shrinkage in cementitious materials. Construct. Build. Mater. 121, 429–436. https://doi.org/10.1016/j.conbuildmat.2016.06.012.
Liu, Y., Schindler, A.K., 2020. Finite-element modeling of early-age concrete stress development. J. Mater. Civil Eng. 32, 04019338 https://doi.org/10.1061/(asce)mt.1943-5533.0002988.
Lokhorst, S.J., 2001. Deformational Behaviour of Concrete Influenced by Hydration Related Changes of the Microstructure. Delft University of Technology.
Loukili, A., Chopin, D., Khelidj, A., Le Touzo, J.-Y., 2000. A new approach to determine autogenous shrinkage of mortar at an early age considering temperature history. Cement Concr. Res. 30, 915–922. https://doi.org/10.1016/S0008-8846(00)00241-6.
Lu, T., Li, Z., Huang, H., 2020a. Effect of supplementary materials on the autogenous shrinkage of cement paste. Materials 13, 1–15. https://doi.org/10.3390/ma13153367.
Lu, T., Li, Z., van Breugel, K., 2020b. Modelling of autogenous shrinkage of hardening cement paste. Construct. Build. Mater. 264 https://doi.org/10.1016/j.conbuildmat.2020.120708.
Lu, T., Li, Z., Huang, H., 2021. Restraining effect of aggregates on autogenous shrinkage in cement mortar and concrete. Construct. Build. Mater. 289, 123166 https://doi.org/10.1016/J.CONBUILDMAT.2021.123166.
Luo, Z., Li, W., Gan, Y., He, X., Castel, A., Sheng, D., 2021. Nanoindentation on micromechanical properties and microstructure of geopolymer with nano-SiO2 and nano-TiO2. Cem. Concr. Compos. 117 https://doi.org/10.1016/j.cemconcomp.2020.103883.
Lura, P., van Breugel, K., Maruyama, I., 2001. Effect of curing temperature and type of cement on early-age shrinkage of high-performance concrete. Cement Concr. Res. 31, 1867–1872. https://doi.org/10.1016/S0008-8846(01)00601-9.
Lura, P., Jensen, O.M., Van Breugel, K., 2003. Autogenous shrinkage in high-performance cement paste: an evaluation of basic mechanisms. Cement Concr. Res. 33, 223–232. https://doi.org/10.1016/S0008-8846(02)00890-6.
Lura, P., Jensen, O.M., Weiss, J., 2009. Cracking in cement paste induced by autogenous shrinkage. Mater. Struct./Mater. Constr. 42, 1089–1099. https://doi.org/10.1617/s11527-008-9445-z.
Di Luzio, G., Cusatis, G., 2009a. Hygro-thermo-chemical modeling of high-performance concrete. II: numerical implementation, calibration, and validation. Cem. Concr. Compos. 31, 309–324. https://doi.org/10.1016/J.CEMCONCOMP.2009.02.016.
Di Luzio, G., Cusatis, G., 2009b. Hygro-thermo-chemical modeling of high performance concrete. I: theory. Cem. Concr. Compos. 31, 301–308. https://doi.org/10.1016/J.CEMCONCOMP.2009.02.015.
Di Luzio, G., Cedolin, L., Beltrami, C., 2020. Tridimensional long-term finite element analysis of reinforced concrete structures with rate-type creep approach. Appl. Sci. 10, 4772. https://doi.org/10.3390/app10144772.
Ma, Y., Yang, X., Hu, J., Zhang, Z., Wang, H., 2019. Accurate determination of the "time-zero" of autogenous shrinkage in alkali-activated fly ash/slag system. Compos. B Eng. 177, 107367 https://doi.org/10.1016/J.COMPOSITESB.2019.107367.
Mallick, S., Anoop, M.B., Balaji Rao, K., 2019a. Early age creep of cement paste - governing mechanisms and role of water-A microindentation study. Cement Concr. Res. 116, 284–298. https://doi.org/10.1016/J.CEMCONRES.2018.12.004.
Mallick, S., Anoop, M.B., Rao, K.B., 2019b. Creep of cement paste containing fly ash - an investigation using microindentation technique. Cement Concr. Res. 121, 21–36. https://doi.org/10.1016/j.cemconres.2019.04.006.
Mao, Y., Liu, J., Shi, C., 2021. Autogenous shrinkage and drying shrinkage of recycled aggregate concrete: a review. J. Clean. Prod. 295, 126435 https://doi.org/10.1016/j.jclepro.2021.126435.
Markandeya, A., Shanahan, N., Gunatilake, D.M., Riding, K.A., Zayed, A., 2018. Influence of slag composition on cracking potential of slag-portland cement concrete. Construct. Build. Mater. 164, 820–829. https://doi.org/10.1016/j.conbuildmat.2017.12.216.
Maruyama, I., Lura, P., 2019. Properties of early-age concrete relevant to cracking in massive concrete. Cement Concr. Res. 123, 105770 https://doi.org/10.1016/J.CEMCONRES.2019.05.015.
Maruyama, I., Teramoto, A., 2013. Temperature dependence of autogenous shrinkage of silica fume cement pastes with a very low water–binder ratio. Cement Concr. Res. 50, 41–50. https://doi.org/10.1016/j.cemconres.2013.03.017.
Mejlhede Jensen, O., Freiesleben Hansen, P., 1995. A dilatometer for measuring autogenous deformation in hardening portland cement paste. Mater. Struct. 28, 406–409. https://doi.org/10.1007/BF02473076.
Moelich, G.M., Kruger, P.J., Combrinck, R., 2022. Mitigating early age cracking in 3D printed concrete using fibres, superabsorbent polymers, shrinkage reducing admixtures, B-CSA cement and curing measures. Cement Concr. Res. 159, 106862 https://doi.org/10.1016/J.CEMCONRES.2022.106862.
Mori, T., Tanaka, K., 1973. Average stress in matrix and average elastic energy of materials with misfitting inclusions. Acta Metall. 21, 571–574. https://doi.org/10.1016/0001-6160(73)90064-3.
Neville, A.M., 2011. Properties of Concrete, fifth ed.
Nguyen, D.H., Nguyen, V.T., Lura, P., Dao, V.T.N., 2019. Temperature-stress testing machine – a state-of-the-art design and its unique applications in concrete research. Cem. Concr. Compos. 102, 28–38. https://doi.org/10.1016/J.CEMCONCOMP.2019.04.019.
Nguyen, Q.D., Afroz, S., Zhang, Y., Kim, T., Li, W., Castel, A., 2022. Autogenous and total shrinkage of limestone calcined clay cement (LC3) concretes. Construct. Build. Mater. 314, 125720 https://doi.org/10.1016/j.conbuildmat.2021.125720.
Orosz, K., Hedlund, H., Cwirzen, A., 2017. Effects of variable curing temperatures on autogenous deformation of blended cement concretes. Construct. Build. Mater. 149, 474–480. https://doi.org/10.1016/j.conbuildmat.2017.05.143.
Ou, G., Lin, Z., Kishi, T., 2023. The practical application of a self-developed temperature stress testing machine in development of expansive concrete blended with calcium sulfoaluminate additives. Cement Concr. Res. 164, 107045 https://doi.org/10.1016/j.cemconres.2022.107045.
Pathirage, M., Bentz, D.P., Di Luzio, G., Masoero, E., Cusatis, G., 2019. The ONIX model: a parameter-free multiscale framework for the prediction of self-desiccation in concrete. Cem. Concr. Compos. 103, 36–48. https://doi.org/10.1016/j.cemconcomp.2019.04.011.
Pichler, C., Lackner, R., Mang, H.A., 2007. A multiscale micromechanics model for the autogenous-shrinkage deformation of early-age cement-based materials. Eng. Fract. Mech. 74, 34–58. https://doi.org/10.1016/j.engfracmech.2006.01.034.
Principagallo, A., Lura, P., Van Breugel, K., Levita, G., 2003. Early development of properties in a cement paste: a numerical and experimental study. Cement Concr. Res. 33, 1013–1020. https://doi.org/10.1016/S0008-8846(03)00002-4.
Raphael, W., Faddoul, R., Geara, F., Chateauneuf, A., 2012. Improvements to the Eurocode 2 shrinkage model for concrete using a large experimental database. Struct. Concr. 13, 174–181. https://doi.org/10.1002/suco.201100029.
Rashid, M.A., Mansur, M.A., Paramasivam, P., 2002. Correlations between mechanical properties of high-strength concrete. J. Mater. Civil Eng. 14, 230–238. https://doi.org/10.1061/(ASCE)0899-1561(2002)14:3(230).
Reinhardt, H.-W., Stegmaier, M., 2006. Influence of heat curing on the pore structure and compressive strength of self-compacting concrete (SCC). Cement Concr. Res. 36, 879–885. https://doi.org/10.1016/j.cemconres.2005.12.004.

Rossi, P., Tailhan, J.L., Le Maou, F., 2013. Comparison of concrete creep in tension and in compression: influence of concrete age at loading and drying conditions. Cement Concr. Res. 51, 78–84. https://doi.org/10.1016/j.cemconres.2013.04.001.
Safiuddin, Md, Kaish, A., Woon, C.-O., Raman, S., 2018. Early-age cracking in concrete: causes, consequences, remedial measures, and recommendations. Appl. Sci. 8, 1730. https://doi.org/10.3390/app8101730.
Sakata, K., Shimomura, T., 2004. Recent progress in research on and code evaluation of concrete creep and shrinkage in Japan. J. Adv. Concr. Technol. 2, 133–140. https://doi.org/10.3151/jact.2.133.
Šavija, B., Zhang, H., Schlangen, E., 2020. Micromechanical testing and modelling of blast furnace slag cement pastes. Construct. Build. Mater. 239 https://doi.org/10.1016/j.conbuildmat.2019.117841.
Schlangen, E., Garboczi, E.J., 1997. Fracture simulations of concrete using lattice models: computational aspects. Eng. Fract. Mech. 57, 319–332. https://doi.org/10.1016/S0013-7944(97)00010-6.
Schröfl, C., Erk, K.A., Siriwatwechakul, W., Wyrzykowski, M., Snoeck, D., 2022. Recent progress in superabsorbent polymers for concrete. Cement Concr. Res. 151, 106648 https://doi.org/10.1016/j.cemconres.2021.106648.
De Schutter, G., 2004. Applicability of degree of hydration concept and maturity method for thermo-visco-elastic behaviour of early age concrete. Cem. Concr. Compos. 26, 437–443. https://doi.org/10.1016/S0958-9465(03)00067-2.
De Schutter, G., Taerwe, L., 2000. Fictitious Degree of Hydration Method for the Basic Creep of Early Age Concrete.
Semianiuk, V., Tur, V., Herrador, M.F., M. Paredes, G., 2017. Early age strains and self-stresses of expansive concrete members under uniaxial restraint conditions. Construct. Build. Mater. 131, 39–49. https://doi.org/10.1016/J.CONBUILDMAT.2016.11.008.
Serdar, M., Gabrijel, I., Schlicke, D., Staquet, S., Azenha, M. (Eds.), 2020. Advanced Techniques for Testing of Cement-Based Materials. Springer International Publishing, Cham. https://doi.org/10.1007/978-3-030-39738-8.
Shen, D., Jiang, J., Shen, J., Yao, P., Jiang, G., 2016. Influence of curing temperature on autogenous shrinkage and cracking resistance of high-performance concrete at an early age. Construct. Build. Mater. 103, 67–76. https://doi.org/10.1016/J.CONBUILDMAT.2015.11.039.
Shen, D., Jiang, J., Wang, W., Shen, J., Jiang, G., 2017. Tensile creep and cracking resistance of concrete with different water-to-cement ratios at early age. Construct. Build. Mater. 146, 410–418. https://doi.org/10.1016/j.conbuildmat.2017.04.056.
Shen, D., Liu, K., Wen, C., Shen, Y., Jiang, G., 2019. Early-age cracking resistance of ground granulated blast furnace slag concrete. Construct. Build. Mater. 222, 278–287. https://doi.org/10.1016/j.conbuildmat.2019.06.028.
Shen, D., Wen, C., Zhu, P., Wu, Y., Yuan, J., 2020a. Influence of Barchip fiber on early-age autogenous shrinkage of high strength concrete. Construct. Build. Mater. 256, 119223 https://doi.org/10.1016/j.conbuildmat.2020.119223.
Shen, D., Jiao, Y., Gao, Y., Zhu, S., Jiang, G., 2020b. Influence of ground granulated blast furnace slag on cracking potential of high performance concrete at early age. Construct. Build. Mater. 241 https://doi.org/10.1016/j.conbuildmat.2019.117839.
Shimomura, T., Maekawa, K., 1997. Analysis of the drying shrinkage behaviour of concrete using a micromechanical model based on the micropore structure of concrete. Mag. Concr. Res. 49, 303–322. https://doi.org/10.1680/macr.1997.49.181.303.
da Silva, W.R.L., Němeček, J., Štemberk, P., 2013. Application of multiscale elastic homogenization based on nanoindentation for high performance concrete. Adv. Eng. Software 62–63, 109–118. https://doi.org/10.1016/j.advengsoft.2013.04.007.
Da Silva, W.R.L., Němeček, J., Štemberk, P., 2014. Methodology for nanoindentation-assisted prediction of macroscale elastic properties of high performance cementitious composites. Cem. Concr. Compos. 45, 57–68. https://doi.org/10.1016/J.CEMCONCOMP.2013.09.013.
Silva, R.V., de Brito, J., Dhir, R.K., 2015. Comparative analysis of existing prediction models on the creep behaviour of recycled aggregate concrete. Eng. Struct. 100, 31–42. https://doi.org/10.1016/j.engstruct.2015.06.004.
Sirtoli, D., Wyrzykowski, M., Riva, P., Tortelli, S., Marchi, M., Lura, P., 2019. Shrinkage and creep of high-performance concrete based on calcium sulfoaluminate cement. Cem. Concr. Compos. 98, 61–73. https://doi.org/10.1016/j.cemconcomp.2019.02.006.
Sirtoli, D., Wyrzykowski, M., Riva, P., Lura, P., 2020. Autogenous and drying shrinkage of mortars based on Portland and calcium sulfoaluminate cements. Mater. Struct. 53, 126. https://doi.org/10.1617/s11527-020-01561-1.
Snoeck, D., Jensen, O.M., De Belie, N., 2015. The influence of superabsorbent polymers on the autogenous shrinkage properties of cement pastes with supplementary cementitious materials. Cement Concr. Res. 74, 59–67. https://doi.org/10.1016/J.CEMCONRES.2015.03.020.
Sorelli, L., Constantinides, G., Ulm, F.J., Toutlemonde, F., 2008. The nano-mechanical signature of Ultra High Performance Concrete by statistical nanoindentation techniques. Cement Concr. Res. 38, 1447–1456. https://doi.org/10.1016/J.CEMCONRES.2008.09.002.
Spingenschmid, R., 1998. Prevention of Thermal Cracking in Concrete at Early Ages. E&FN Spon, London.
Springenschmid, R., Breitenbücher, R., Mangold, M., 1994. Development of the cracking frame and the temperature-stress testing machine. In: Proceedings of the International RILEM Symposium, Munich, Germany, pp. 137–144.
Staquet, S., Delsaute, B., Darquennes, A., Espion, B., 2012. Design of a revisited TSTM system for testing concrete since setting time under free and restraint conditions. In: CONCRACK 3 – RILEM-JCI International Workshop on Crack Control of Mass Concrete and Related Issues Concerning Early-Age of Concrete Structures, Paris, France.
Sun, M., Visintin, P., Bennett, T., 2022a. The effect of specimen size on autogenous and total shrinkage of ultra-high performance concrete (UHPC). Construct. Build. Mater. 327, 126952 https://doi.org/10.1016/J.CONBUILDMAT.2022.126952.
Sun, Y., Lu, J.-X., Poon, C.S., 2022b. Strength degradation of seawater-mixed alite pastes: an explanation from statistical nanoindentation perspective. Cement Concr. Res. 152, 106669 https://doi.org/10.1016/j.cemconres.2021.106669.
Suwanmaneechot, P., Aili, A., Maruyama, I., 2020. Creep behavior of C-S-H under different drying relative humidities: interpretation of microindentation tests and sorption measurements by multi-scale analysis. Cement Concr. Res. 132 https://doi.org/10.1016/j.cemconres.2020.106036.
Tang, S., Huang, D., He, Z., 2021. A review of autogenous shrinkage models of concrete. J. Build. Eng. 44, 103412 https://doi.org/10.1016/j.jobe.2021.103412.
Tazawa, E., Miyazawa, S., 1995. Influence of cement and admixture on autogenous shrinkage of cement paste. Cement Concr. Res. 25, 281–287. https://doi.org/10.1016/0008-8846(95)00010-0.
Tennis, P.D., Jennings, H.M., 2000. A model for two types of calcium silicate hydrate in the microstructure of Portland cement pastes. Cement Concr. Res. 30, 855–863. https://doi.org/10.1016/S0008-8846(00)00257-X.
Torrenti, J.M., Le Roy, R., 2018. Analysis of some basic creep tests on concrete and their implications for modeling. Struct. Concr. 19, 483–488. https://doi.org/10.1002/suco.201600197.
Tran, N.P., Gunasekara, C., Law, D.W., Houshyar, S., Setunge, S., Cwirzen, A., 2021. A critical review on drying shrinkage mitigation strategies in cement-based materials. J. Build. Eng. 38, 102210 https://doi.org/10.1016/j.jobe.2021.102210.
Valcuende, M., Marco, E., Parra, C., Serna, P., 2012. Influence of limestone filler and viscosity-modifying admixture on the shrinkage of self-compacting concrete. Cement Concr. Res. 42, 583–592. https://doi.org/10.1016/j.cemconres.2012.01.001.
Vandamme, M., Ulm, F.-J., 2013. Nanoindentation investigation of creep properties of calcium silicate hydrates. Cement Concr. Res. 52, 38–52. https://doi.org/10.1016/j.cemconres.2013.05.006.
Viviani, M., Glisic, B., Smith, I.F.C., 2007. Separation of thermal and autogenous deformation at varying temperatures using optical fiber sensors. Cem. Concr. Compos. 29, 435–447. https://doi.org/10.1016/j.cemconcomp.2007.01.005.
Waller, V., d'Aloïa, L., Cussigh, F., Lecrux, S., 2004. Using the maturity method in concrete cracking control at early ages. Cem. Concr. Compos. 26, 589–599. https://doi.org/10.1016/S0958-9465(03)00080-5.
Wang, W., Gong, J., 2019. New relaxation function and age-adjusted effective modulus expressions for creep analysis of concrete structures. Eng. Struct. 188, 1–10. https://doi.org/10.1016/j.engstruct.2019.03.009.
Wang, L., Li, G., Li, X., Guo, F., Tang, S., Lu, X., Hanif, A., 2022. Influence of reactivity and dosage of MgO expansive agent on shrinkage and crack resistance of face slab concrete. Cem. Concr. Compos. 126, 104333 https://doi.org/10.1016/j.cemconcomp.2021.104333.
Wei, Y., Liang, S., Gao, X., 2017a. Indentation creep of cementitious materials: experimental investigation from nano to micro length scales. Construct. Build. Mater. 143, 222–233. https://doi.org/10.1016/j.conbuildmat.2017.03.126.
Wei, Y., Liang, S., Guo, W., Hansen, W., 2017b. Stress prediction in very early-age concrete subject to restraint under varying temperature histories. Cem. Concr. Compos. 83, 45–56. https://doi.org/10.1016/j.cemconcomp.2017.07.006.
Wei, Y., Wu, Z., Huang, J., Liang, S., 2018. Comparison of compressive, tensile, and flexural creep of early-age concretes under sealed and drying conditions. J. Mater. Civil Eng. 30, 04018289 https://doi.org/10.1061/(asce)mt.1943-5533.0002495.
Wei, Y., Huang, J., Liang, S., 2020. Measurement and modeling concrete creep considering relative humidity effect. Mech. Time-Depend. Mater. 24, 161–177. https://doi.org/10.1007/s11043-019-09414-3.
Wilson, W., Rivera-Torres, J.M., Sorelli, L., Durán-Herrera, A., Tagnit-Hamou, A., 2017. The micromechanical signature of high-volume natural pozzolan concrete by combined statistical nanoindentation and SEM-EDS analyses. Cement Concr. Res. 91, 1–12. https://doi.org/10.1016/J.CEMCONRES.2016.10.004.
Wilson, W., Sorelli, L., Tagnit-Hamou, A., 2018. Unveiling micro-chemo-mechanical properties of C–(A)–S–H and other phases in blended-cement pastes. Cement Concr. Res. 107, 317–336. https://doi.org/10.1016/J.CEMCONRES.2018.02.010.
Wittmann, F., 1974. Bestimmung physikalischer Eigenschaften des Zementsteins.
Wu, L., Farzadnia, N., Shi, C., Zhang, Z., Wang, H., 2017. Autogenous shrinkage of high performance concrete: a review. Construct. Build. Mater. 149, 62–75. https://doi.org/10.1016/j.conbuildmat.2017.05.064.
Wyrzykowski, M., Hu, Z., Ghourchian, S., Scrivener, K., Lura, P., 2017. Corrugated tube protocol for autogenous shrinkage measurements: review and statistical assessment. Mater. Struct. 50, 57. https://doi.org/10.1617/s11527-016-0933-2.
Wyrzykowski, M., Scrivener, K., Lura, P., 2019. Basic creep of cement paste at early age - the role of cement hydration. Cement Concr. Res. 116, 191–201. https://doi.org/10.1016/j.cemconres.2018.11.013.
Xin, J., Zhang, G., Liu, Y., Wang, Z., Wu, Z., 2020. Evaluation of behavior and cracking potential of early-age cementitious systems using uniaxial restraint tests: a review. Construct. Build. Mater. 231, 117146 https://doi.org/10.1016/J.CONBUILDMAT.2019.117146.
Xin, J., Liu, Y., Zhang, G., Wang, Z., Yang, N., Qiao, Y., Wang, J., 2021. Comparison of thermal cracking potential evaluation criteria for mass concrete structures. Mater. Struct. 54, 243. https://doi.org/10.1617/s11527-021-01840-5.
Xin, J., Liu, Y., Zhang, G., Wang, Z., Wang, J., Yang, N., Qiao, Y., 2022. Evaluation of early-age thermal cracking resistance of high w/b, high volume fly ash (HVFA) concrete using temperature stress testing machine. Case Stud. Constr. Mater. 16, e00825 https://doi.org/10.1016/j.cscm.2021.e00825.
Yang, J., Wang, Q., Zhou, Y., 2017. Influence of curing time on the drying shrinkage of concretes with different binders and water-to-binder ratios. Adv. Mater. Sci. Eng. 2017, 1–10. https://doi.org/10.1155/2017/2695435.

Yang, L., Shi, C., Wu, Z., 2019. Mitigation techniques for autogenous shrinkage of ultra-high-performance concrete – a review. Compos. B Eng. 178, 107456 https://doi.org/10.1016/J.COMPOSITESB.2019.107456.

Ye, G., van Breugel, K., Fraaij, A.L.A., 2003. Three-dimensional microstructure analysis of numerically simulated cementitious materials. Cement Concr. Res. 33, 215–222. https://doi.org/10.1016/S0008-8846(02)00889-X.

Yu, Q., Bažant, P., Wendner, R., 2012. Improved algorithm for efficient and realistic creep analysis of large creep-sensitive concrete structures. ACI Struct. J. 109 https://doi.org/10.14359/51684044.

Yu, P., Duan, Y.H., Fan, Q.X., Tang, S.W., 2020. Improved MPS model for concrete creep under variable humidity and temperature. Construct. Build. Mater. 243, 118183 https://doi.org/10.1016/j.conbuildmat.2020.118183.

B.P. Zdenek Bazant, S. Prasannan, S. Member, SOLIDIFICATION THEORY FOR CONCRETE CREEP. II: VERIFICATION AND APPLICATION, (n.d).

Zhan, P., He, Z., 2019. Application of shrinkage reducing admixture in concrete: a review. Construct. Build. Mater. 201, 676–690. https://doi.org/10.1016/j.conbuildmat.2018.12.209.

Zhang, M.H., Tam, C.T., Leow, M.P., 2003. Effect of water-to-cementitious materials ratio and silica fume on the autogenous shrinkage of concrete. Cement Concr. Res. 33, 1687–1694. https://doi.org/10.1016/S0008-8846(03)00149-2.

Zhang, Q., Le Roy, R., Vandamme, M., Zuber, B., 2014. Long-term creep properties of cementitious materials: comparing microindentation testing with macroscopic uniaxial compressive testing. Cement Concr. Res. 58, 89–98. https://doi.org/10.1016/J.CEMCONRES.2014.01.004.

Zhang, H., Šavija, B., Figueiredo, S.C., Schlangen, E., 2017. Experimentally validated multi-scale modelling scheme of deformation and fracture of cement paste. Cement Concr. Res. 102, 175–186. https://doi.org/10.1016/J.CEMCONRES.2017.09.011.

Zhang, X., Liu, Z., Wang, F., 2019a. Autogenous shrinkage behavior of ultra-high performance concrete. Construct. Build. Mater. 226, 459–468. https://doi.org/10.1016/j.conbuildmat.2019.07.177.

Zhang, H., Šavija, B., Luković, M., Schlangen, E., 2019b. Experimentally informed micromechanical modelling of cement paste: an approach coupling X-ray computed tomography and statistical nanoindentation. Compos. B Eng. 157, 109–122. https://doi.org/10.1016/J.COMPOSITESB.2018.08.102.

Zhang, H., Xu, Y., Gan, Y., Chang, Z., Schlangen, E., Šavija, B., 2020. Microstructure informed micromechanical modelling of hydrated cement paste: techniques and challenges. Construct. Build. Mater. 251, 118983 https://doi.org/10.1016/J.CONBUILDMAT.2020.118983.

Zhang, B., Zhu, H., Feng, P., Zhang, P., 2022a. A review on shrinkage-reducing methods and mechanisms of alkali-activated/geopolymer systems: effects of chemical additives. J. Build. Eng. 49, 104056 https://doi.org/10.1016/j.jobe.2022.104056.

Zhang, W., Lin, H., Xue, M., Wang, S., Ran, J., Su, F., Zhu, J., 2022b. Influence of shrinkage reducing admixtures on the performance of cementitious composites: a review. Construct. Build. Mater. 325, 126579 https://doi.org/10.1016/j.conbuildmat.2022.126579.

Zhang, W., Lin, H., Xue, M., Wang, S., Ran, J., Su, F., Zhu, J., 2022c. Influence of shrinkage reducing admixtures on the performance of cementitious composites: a review. Construct. Build. Mater. 325, 126579 https://doi.org/10.1016/j.conbuildmat.2022.126579.

Zhang, J., Ma, Y., Zhao, H., Sun, H., Liu, J., 2022d. Mitigating autogenous shrinkage of cement paste with novel shrinkage-reducing polycarboxylate superplasticizer. Mater. Struct. 55, 231. https://doi.org/10.1617/s11527-022-02066-9.

Zhao, H., Liu, J., Yin, X., Wang, Y., Huang, D., 2019a. A multiscale prediction model and simulation for autogenous shrinkage deformation of early-age cementitious materials. Construct. Build. Mater. 215, 482–493. https://doi.org/10.1016/j.conbuildmat.2019.04.225.

Zhao, Z., Wang, K., Lange, D.A., Zhou, H., Wang, W., Zhu, D., 2019b. Creep and thermal cracking of ultra-high volume fly ash mass concrete at early age. Cem. Concr. Compos. 99, 191–202. https://doi.org/10.1016/j.cemconcomp.2019.02.018.

Zhao, Z., Zhang, H., Fang, B., Sun, Y., Zhong, Y., Shi, T., 2020. Tensile creep model of slab concrete based on microprestress-solidification theory. Materials 13, 3157. https://doi.org/10.3390/ma13143157.

Zhao, H., Liu, H., Wan, Y., Maria Ghantous, R., Li, J., Liu, Y., Ni, Y., Guan, J., 2021. Mechanical properties and autogenous deformation behavior of early-age concrete containing pre-wetted ceramsite and CaO-based expansive agent. Construct. Build. Mater. 267 https://doi.org/10.1016/j.conbuildmat.2020.120992.

Zhao, H., Xiang, Y., Liu, J., Zhang, Z., Jia, R., Yao, T., Li, H., Xu, W., Tian, Q., 2022. Effects of reinforcement on autogenous deformation of early-age concrete containing CaO-based expansion agent. Construct. Build. Mater. 320, 126197 https://doi.org/10.1016/j.conbuildmat.2021.126197.

Zheng, X., Ji, T., Easa, S.M., Zhang, B., Jiang, Z., 2019. Tensile basic creep behavior of lightweight aggregate concrete reinforced with steel fiber. Construct. Build. Mater. 200, 356–367. https://doi.org/10.1016/j.conbuildmat.2018.12.138.

Zhou, F.P., Lydon, F.D., Barr, B.I.G., 1995. Effect of coarse aggregate on elastic modulus and compressive strength of high performance concrete. Cement Concr. Res. 25, 177–186. https://doi.org/10.1016/0008-8846(94)00125-I.

Zhu, H., Li, Q., Hu, Y., Ma, R., 2018. Double feedback control method for determining early-age restrained creep of concrete using a temperature stress testing machine. Materials 11. https://doi.org/10.3390/ma11071079.

Zhu, L., Wang, J.-J., Li, X., Zhao, G.-Y., Huo, X.-J., 2020a. Experimental and numerical study on creep and shrinkage effects of ultra high-performance concrete beam. Compos. B Eng. 184, 107713 https://doi.org/10.1016/j.compositesb.2019.107713.

Zhu, H., Hu, Y., Li, Q., Ma, R., 2020b. Restrained cracking failure behavior of concrete due to temperature and shrinkage. Construct. Build. Mater. 244, 118318 https://doi.org/10.1016/j.conbuildmat.2020.118318.

Zhu, H., Hu, Y., Ma, R., Wang, J., Li, Q., 2021. Concrete thermal failure criteria, test method, and mechanism: a review. Construct. Build. Mater. 283, 122762 https://doi.org/10.1016/j.conbuildmat.2021.122762.

Zhuang, Y., Zheng, D., Ng, Z., Ji, T., Chen, X., 2016. Effect of lightweight aggregate type on early-age autogenous shrinkage of concrete. Construct. Build. Mater. 120, 373–381. https://doi.org/10.1016/j.conbuildmat.2016.05.105.

Zhutovsky, S., Kovler, K., Bentur, A., 2002. Efficiency of lightweight aggregates for internal curing of high strength concrete to eliminate autogenous shrinkage. Mater. Struct. 35, 97–101. https://doi.org/10.1007/BF02482108.

Šmilauer, V., Bittnar, Z.Ǩ, 2006. Microstructure-based micromechanical prediction of elastic properties in hydrating cement paste. Cement Concr. Res. 36, 1708–1718. https://doi.org/10.1016/j.cemconres.2006.05.014.